

Background from K_L^0 decays upstream of the decay region

David E. Jaffe, BNL

June 8, 2005

Abstract

Background from single $K_L^0 \rightarrow \pi^0\pi^0\pi^0$ and $K_L^0 \rightarrow \pi^0\pi^0$ decays as well as pairs of K_L^0 decays upstream of the decay region is studied using the FastMC. These studies show the background can be reduced to negligible levels with a cut on the measured photon conversion position with a loss of signal of 9% for the 2γ PR detection method.

1 Introduction

K_L^0 decays upstream of the decay region can produce significant background due to the combination of two effects.

1. When the photon candidates are not the product of a single π^0 decay, then the apparent K_L^0 decay point can be mis-reconstructed downstream of the actual K_L^0 decay point.
2. If the K_L^0 decays far enough upstream of the decay region, then none of the other K_L^0 decay products will register in a veto detector.

The FastMC was used to investigate this background. It is dominated by single $K_L^0 \rightarrow \pi^0\pi^0\pi^0$ decays where an 'odd' photon pair is mis-reconstructed. Single $K_L^0 \rightarrow \pi^0\pi^0$ decays also contribute to this background but are suppressed by the Kp2 decay rate. In principle, $K_L^0 \rightarrow e^\pm\pi^\mp\nu\gamma$ decays could also contribute. This contribution has not been studied yet, mainly because it takes an excessive amount of CPU time to generate $K_L^0 \rightarrow e^\pm\pi^\mp\nu\gamma$ decays using the brute force 'acceptance/rejection' method for the Ke3g matrix element in the FastMC.

Background from pairs of K_L^0 decays upstream of the decay region are heavily suppressed by the relative rate and by the probability that other decay products will veto the event.

2 Assumptions and data samples

This note deals only with the 2γ PR detection method.

If units are omitted from a figure or text, assume centimeters, nanoseconds, or MeV as appropriate. Other notation: Kp3 is $K_L^0 \rightarrow \pi^0\pi^0\pi^0$, Kp2 is $K_L^0 \rightarrow \pi^0\pi^0$, Ke3g is $K_L^0 \rightarrow e^\pm\pi^\mp\nu\gamma$ and Kpnn is signal.

The geometry of the detector as simulated in the FastMC [1] is given in Table 1.

I assume that potential signal candidate photons that strike the beam pipe will not strike the PR or CAL. In reality some fraction of photons that strike the pipe will

X halfwidth	Y halfwidth	Z at US end	Z at DS end	Volume name
92.50	5.00	-10.0	997.0	Beam pipe
127.00	127.00	997.0	1397.0	Decay vol
150.00	150.00	1397.0	1531.0	Pre-Rad
220.00	220.00	1531.0	1601.0	Calorim
92.50	16.00	1397.0	1601.0	DS hole
200.00	50.00	1601.0	2596.0	CatchrVol
150.00	15.00	2596.0	2596.0	Catcher detector (special)

Table 1: FastMC definition of the detector. Units are centimeters. The y aperture of the US and DS beam pipe differ from that used for the April 2005 Baseline Review. The “DS hole” is interpreted as the the inner limits of the PR active area in the FastMC.

either not interact and reach the PR or CAL, or interact but send a photon or photons into the PR or CAL. The effect of this assumption is discussed in Section 6.

The upstream veto wall (UV) is crucial in rejecting background from upstream (US) decays. For this study, I assume that the UV extends 80 cm upstream of the decay region ($917 < z < 997$ cm)¹ and that tracks (both photons and charged particles) that strike the beam pipe with $z > 917$ cm can be vetoed by the UV. Tracks which strike the beam pipe with $z < 917$ cm are assumed to have a veto efficiency of zero. The latter assumption is known to be conservative; a GEANT3 study demonstrated that K_L^0 decays ~ 150 cm upstream of the UV have non-zero veto efficiency (see Figure 14 of [2]).

For photons that strike the beam pipe in the region $917 < z < 997$ cm, the photon veto (PV) inefficiency takes into account degradation of the PV due to the incident angle dependence on the 0.25” thick Al beam pipe. For charged pions that strike the beam pipe in the region $917 < z < 997$ cm, the charged pion veto inefficiency is degraded by assuming the charged pion must traverse 0.25” of aluminum before reaching the UV. The incidence angle is ignored for the CPV inefficiency because in the model used to assign the CPV inefficiency in the FastMC, I assume that photons from pion interactions will be detectable in the PV that ‘backs-up’ the CPV.

Two separate samples of $K_L^0 \rightarrow \pi^0\pi^0\pi^0$ and $K_L^0 \rightarrow \pi^0\pi^0$ decays were generated with decay points in the range $47 < z < 997$ cm. The first sample comprised 5×10^8 $K_L^0 \rightarrow \pi^0\pi^0\pi^0$ and 5×10^8 $K_L^0 \rightarrow \pi^0\pi^0$ decays and was used to study and set cuts. The second sample comprised 3×10^8 events of each decay mode and was used to measure the rejection of the cuts. The region $47 < z < 997$ cm corresponds to the beam pipe volume from the spoiler to the US end of the decay region. Events with exactly two photons striking the PR and no other photons striking the barrel veto were accepted for further analysis (This is called the “Trigger” requirement in Table 2). These pairs of photons were subjected to the standard reconstruction algorithm and then loose ‘skim’ cuts were applied. The number of generated and accepted events are given in Table 2. The skim cuts were $-10 < z(K_L^0) < 2000$ cm, $M_{\gamma\gamma} < 300$ MeV/ c^2 , and $E^*(\pi^0) < 1000$ MeV.

A sample of 7×10^8 pairs of K_L^0 decays were generated with decay points in the range $47 < z < 997$ cm. For this sample, each K_L^0 was allowed to decay freely according to the known branching fractions. The “trigger” for these events required exactly two photons and no other particles to exit from DS aperture of the beam pipe at $z = 997$ cm. The same “skim” requirements listed above were applied. The number of generated and accepted events are given in Table 2. I did not generate another sample of pairs of K_L^0 decays because I did not change the cuts based on this sample.

¹The UV extends 76.8 cm upstream of the decay region as described in the CDR.

	$K_L^0 \rightarrow \pi^0\pi^0\pi^0$		$K_L^0 \rightarrow \pi^0\pi^0$		$2 K_L^0$	
	Events	Fraction	Events	Fraction	Events	Fraction
Generated	500000000		500000000		300000000	
Triggers	2083589	0.417%	1459508	0.292%	150499	0.050%
Skimmed	2036076	0.407%	1386409	0.277%	144462	0.0482%

Table 2: Generated events and fraction accepted by “trigger” and “skim” requirements. $K_L^0 \rightarrow \pi^0\pi^0\pi^0$ and $K_L^0 \rightarrow \pi^0\pi^0$ are single K_L^0 decays generated US of the decay region. $2 K_L^0$ are pairs of K_L^0 decays generated US of the decay region with the K_L^0 allowed to decay freely according to the known branching fractions.

3 Cuts

The cuts are denoted by five letter acronyms and defined below. The cuts are classified as “GeomAcc”, “GoodFit”, “Fiducial”, “MisRecon”, “Kinematic” and “Likelihood”. The description of the cuts given below corresponds to the 2γ PR detection method only.

The order of the cuts listed below is the sequence in which they are applied.

- o GeomAcc : Geometric acceptance
 1. **Accpt** Each photon must be within the barrel radius at the front of the PR and must be outside the DS beam hole at the front of the calorimeter
- o GoodFit : Good fit
 1. **Ierr** Reconstruction algorithm and fitting procedure must be successful; that is, both fits must converge within 20 iterations. Recall that two sequential fits are performed in the FastMC. The first fit requires the photons to originate from a common vertex in space and time within the y -beam envelope. The second, and final, fit adds the constraint of the π^0 mass.
 2. **ValKL** Reconstructed K_L^0 candidate must be physically valid: $\beta(K_L^0) < 1$.
 3. **Chi2n** The χ^2 of the first fit must be < 100 . See Figure 1.
- o Fiducial : Reconstructed K_L^0 candidate and photon candidates must pass “fiducial” cuts.
 1. **delT** The time of the two photons extrapolated to the reconstructed K_L^0 vertex must be within ± 1 ns : $|t_{\gamma 1} - t_{\gamma 2}| < 1$ ns. See Figure 2.
 2. **XK** The x -position of the K_L^0 candidate must be near the beam envelope : $|x(K_L^0)| < 75$ cm. This cut was originally designed to suppress background from pion beta decay because π^\pm frequently leave the beam envelope before decay. See Figure 3.
 3. **YK** The y -position of the K_L^0 candidate must be near the beam envelope : $|y(K_L^0)| - \Delta y/2 \times z(K_L^0) < 2$ cm and $z(K_L^0) > 1075 \times (|y(K_L^0)|/1.5)^{0.2}$ where Δy is the vertical beam aspect ratio. The first requirement was originally designed to suppress background from pion beta decay. The second requirement is based on the distribution of candidates from US $K_L^0 \rightarrow \pi^0\pi^0\pi^0$ decays compared to signal decays. See Figure 4.
 4. **ZK** The z -position of the K_L^0 candidate must be far from the ends of the decay volume : $1072 < z(K_L^0) < 1347$ cm. This requirement was originally designed to suppress background from the $nN \rightarrow \pi^0 X$ process in the material at the ends of the decay volume. It also suppresses background from US K_L^0 decays. See Figure 5.

5. **YatCL** The maximum y -position of the reconstructed photon at the US face of the calorimeter : $\max(|y_{\gamma_1}|, |y_{\gamma_2}|) > 50$ cm. In the real data, we would probably cut on the y -position of the conversion point in the PR as a function of z of the conversion point; however, in the FastMC, photons are not converted at a point but are treated on a statistical basis. The “true” (unsmearred) y -position of the photon extrapolated to the front of the calorimeter is used as an approximation to y of the conversion point. The unsmearred trajectory of the photon is used because the y resolution in the PR of the conversion point is expected to be a few hundred microns. This cut is specifically designed to suppress background from K_L^0 decays US of the decay region. Figure 6 shows $\max(|y_{\gamma_1}|, |y_{\gamma_2}|)$ vs $\min(|y_{\gamma_1}|, |y_{\gamma_2}|)$ without and with event weighting. Figure 7 shows $\max(|y_{\gamma_1}|, |y_{\gamma_2}|)$ vs the true z position of the K_L^0 decay.
- **MisRecon** : Cuts designed to suppress background from “mis-reconstructed” events. These were originally designed to suppress $Kp2$ -odd and $K_L^0 \rightarrow e^\pm \pi^\mp \nu \gamma$ backgrounds where the reconstructed $z(K_L^0)$ was far downstream of the true K_L^0 decay point.
 1. **DOCA** The distance of the closest approach of the two measured photons must be within 60 cm. See Figure 8.
 2. **DK12** $DK12 \equiv \sqrt{(z(K_L^0, \text{fit1}) - z(K_L^0, \text{fit2}))^2 + (\text{DOCA1} + \text{DOCA2} - 5.)^2} < 30$ cm where $z(K_L^0, \text{fit}i)$ is the reconstructed z of the K_L^0 candidate from the i^{th} fit and $\text{DOCA}i$ is the distance of closest approach of the i^{th} measured photon to the K_L^0 vertex from the second fit. For mis-reconstructed candidates, the measured energy and the π^0 mass constraint displace the vertex of the second fit with respect to the first fit. DK12 attempts to exploit this feature. See Figure 9.
 3. **sgZK1** The calculated uncertainty on $z(K_L^0, \text{fit1})$ must be less than 25 cm. See Figure 10.
 - **Kinematic** : Basic kinematic cuts to suppress background and to facilitate the likelihood cut.
 1. **PK** The reconstructed three momentum of the K_L^0 must be > 400 MeV/ c . This cut suppresses background from K_L^0 decays from the next microbunch. See Figure 11.
 2. **Eg** The minimum photon energy must satisfy $E_\gamma > \min(100, \max(2\chi^2, \min(70, 20 + 5\chi^2)))$ MeV where χ^2 is the chi-squared value from the first fit. This cut is designed to suppress background from Michel electrons from stopped muon decays being interpreted as photons.
 3. **Mnu2** $(p(K_L^0) - p(\pi^0) - p(\pi))^2 < -30000$ MeV² where $p(K_L^0)$ and $p(\pi^0)$ are the reconstructed four-momentum of the K_L^0 and π^0 candidate and $p(\pi)$ is taken to be the charged pion mass. This cut is designed to suppress slow charged tracks from K_L^0 decays that would fall far outside the veto timing gates.
 4. **Mgg** The reconstructed mass of the two photons from the first fit must satisfy $-30 < M(\gamma\gamma) - M(\pi^0) < 40$ MeV/ c^2 . This cut suppress background when the two photons do not originate from a single π^0 . See Figure 12.
 5. **E*pi** The energy of the reconstructed π^0 candidate in the K_L^0 rest frame must be less than 300 MeV. This cut suppress background from non- K_L^0 sources.

○ Likelihood : The 3-dimensional optimized cut on $M(\gamma\gamma) - M(\pi^0)$, $T^{*2} \equiv$ the square of the kinetic energy of the π^0 candidate in the K_L^0 rest frame and $\ln(E_{\text{miss}})$ where E_{miss} is the missing energy of the K_L^0 candidate in the lab. See Figure 13.

1. Like The likelihood cut chosen for this note is rather loose as can be seen from the distribution in Figure 13.

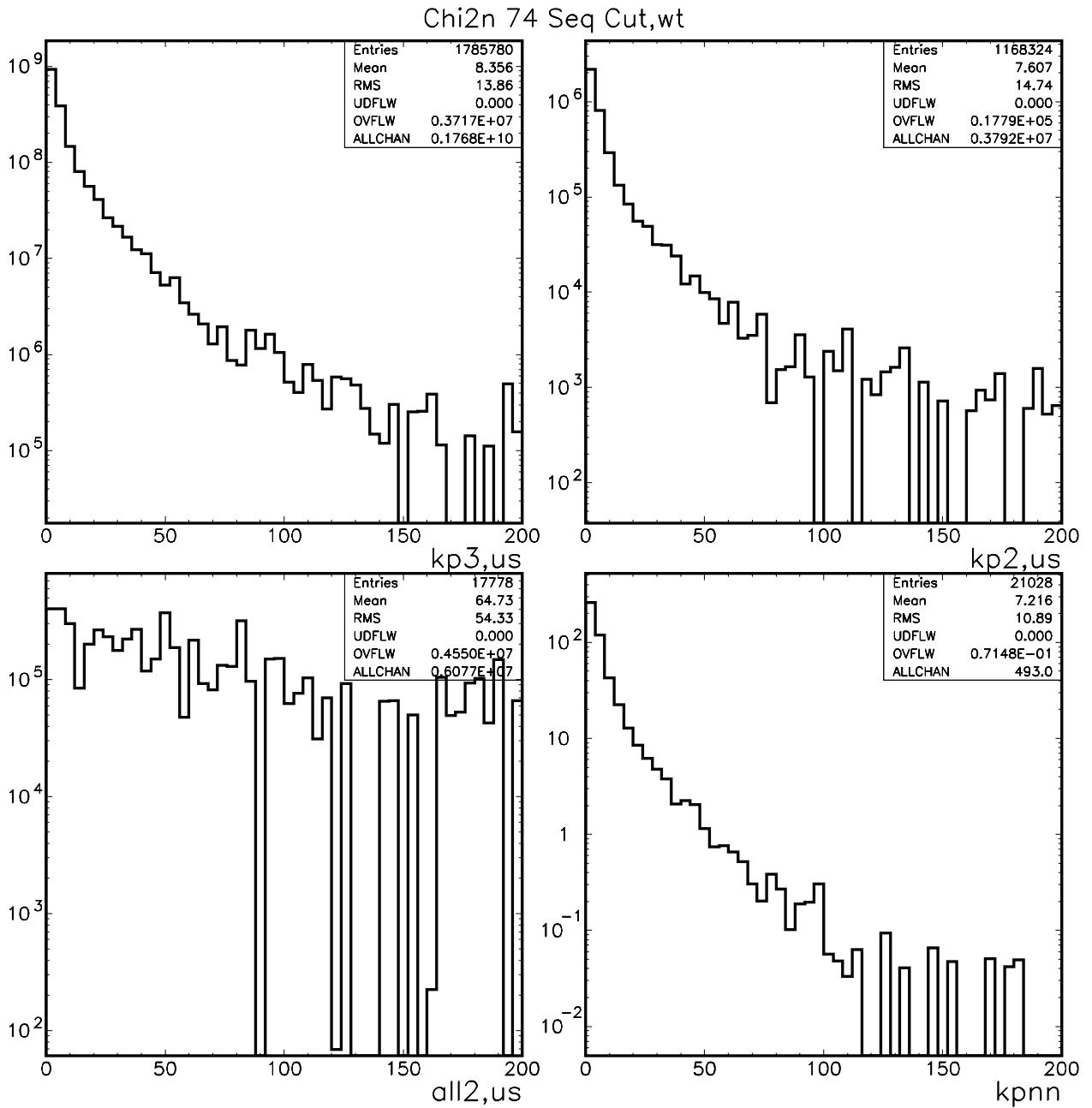


Figure 1: Distribution of Chi2n for $K_L^0 \rightarrow \pi^0\pi^0\pi^0$, $K_L^0 \rightarrow \pi^0\pi^0$, signal and $2K_L^0$ decays clockwise from top left. All cuts prior to the cuts on this distribution are applied. The distributions are weighted.

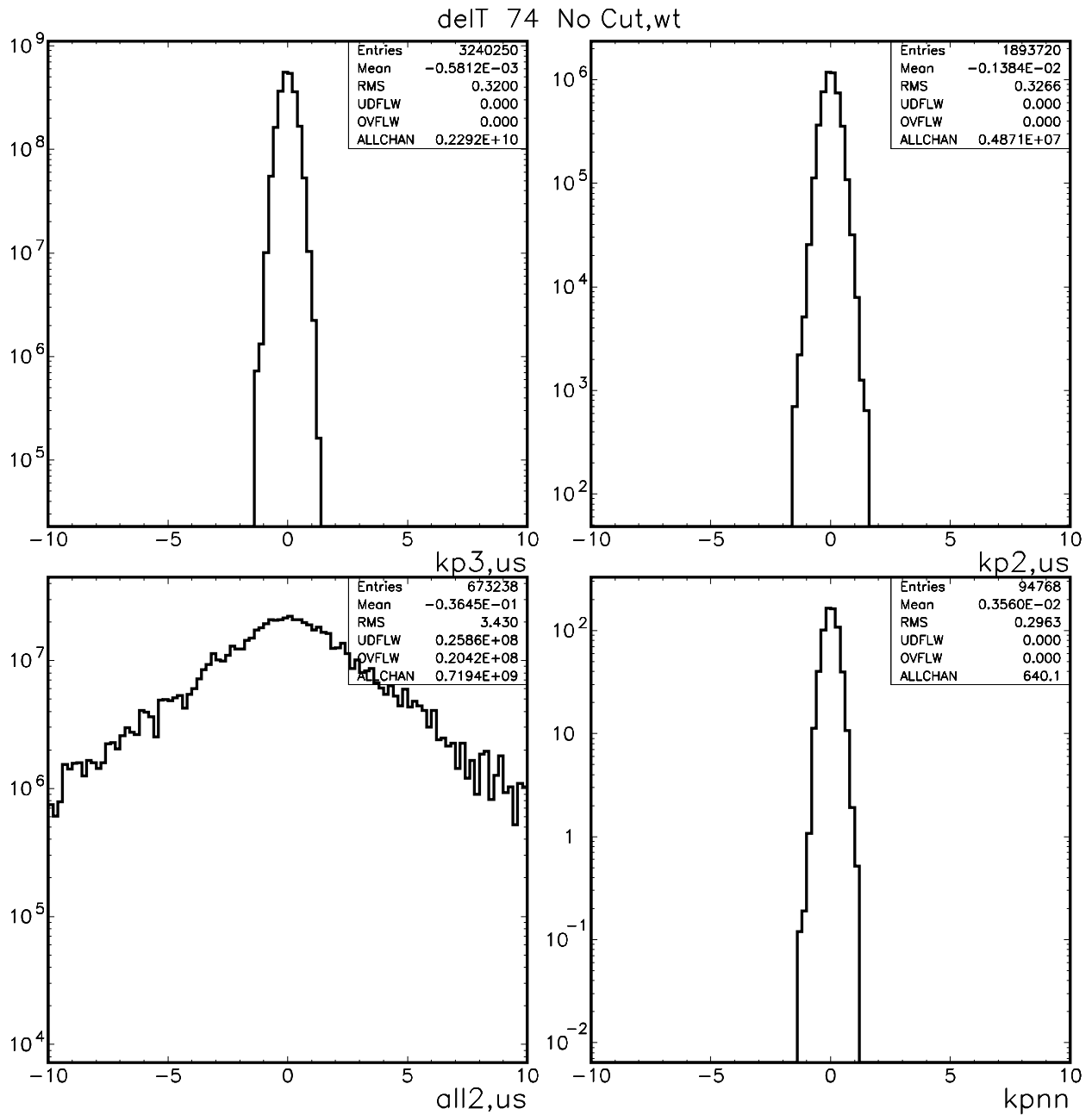


Figure 2: Distribution of $deIT$ for $K_L^0 \rightarrow \pi^0\pi^0\pi^0$, $K_L^0 \rightarrow \pi^0\pi^0$, signal and $2K_L^0$ decays clockwise from top left. No cuts have been applied. The distributions are weighted.

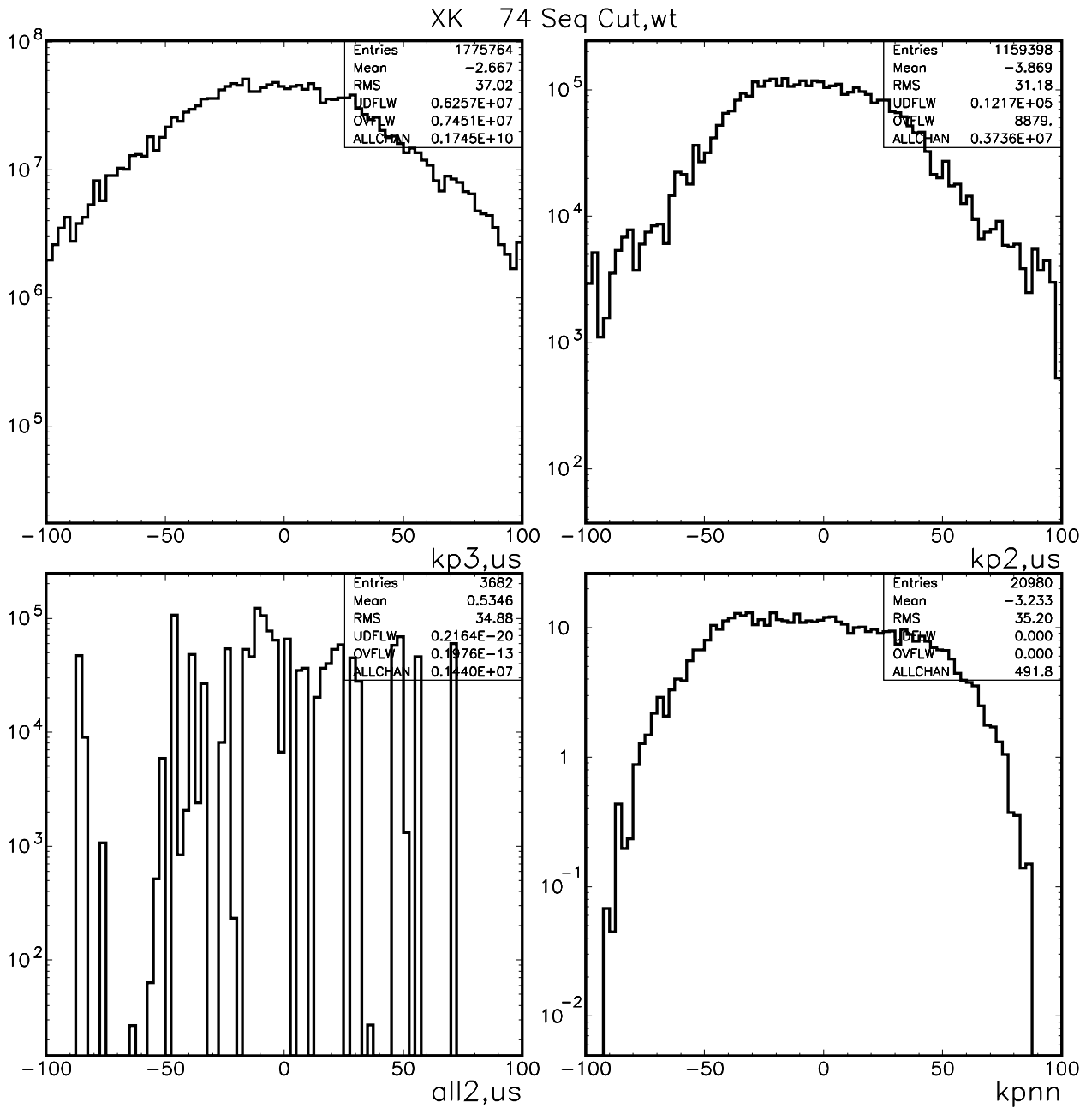


Figure 3: Distribution of XK for $K_L^0 \rightarrow \pi^0 \pi^0 \pi^0$, $K_L^0 \rightarrow \pi^0 \pi^0$, signal and $2K_L^0$ decays clockwise from top left. All cuts prior to the cuts on this distribution are applied. The distributions are weighted.

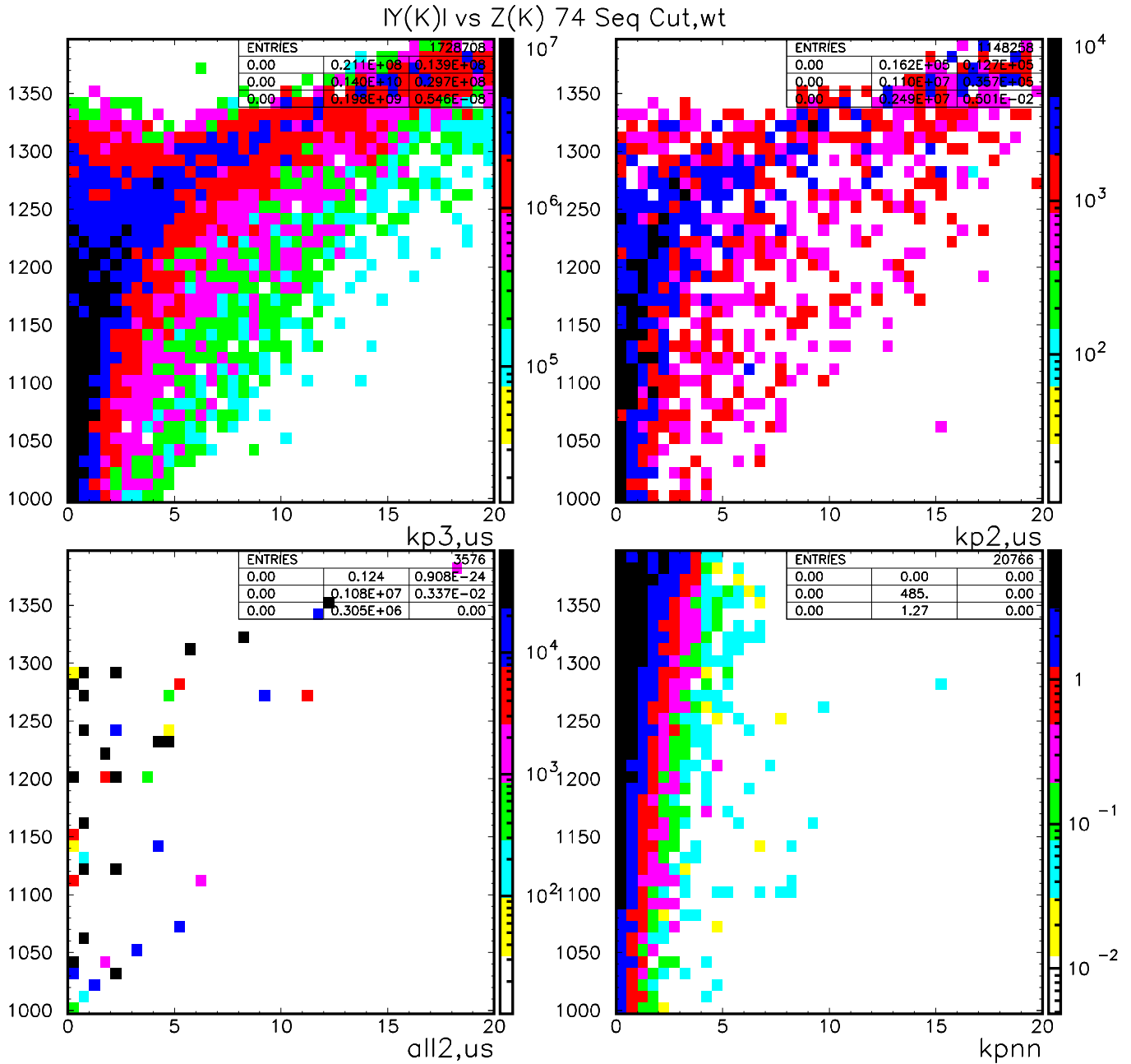


Figure 4: Distribution of $|y(K_L^0)|$ vs $z(K_L^0)$ for $K_L^0 \rightarrow \pi^0 \pi^0 \pi^0$, $K_L^0 \rightarrow \pi^0 \pi^0$, signal and $2K_L^0$ decays clockwise from top left. All cuts prior to the cuts on this distribution are applied. The distributions are weighted.

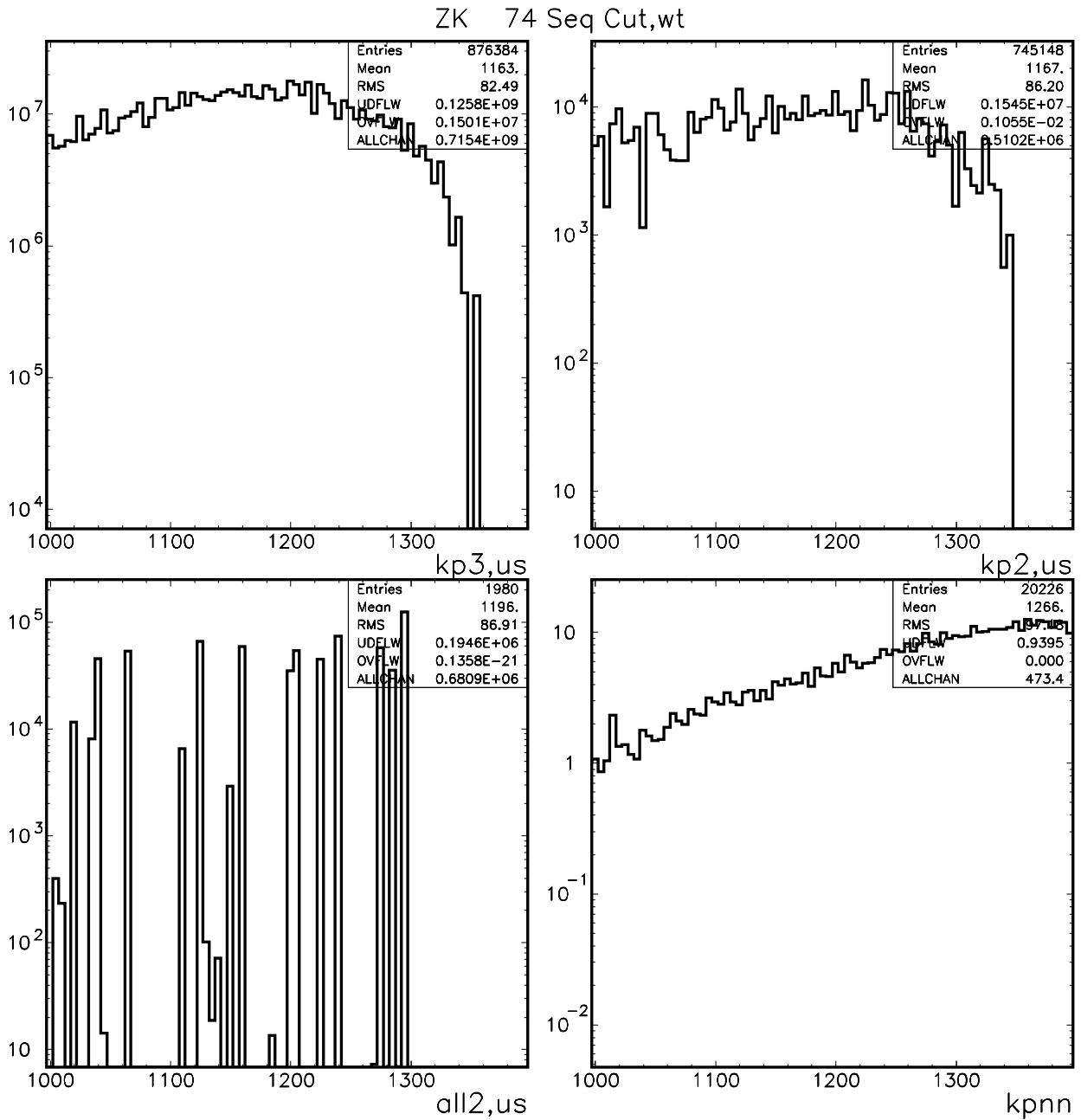


Figure 5: Distribution of ZK for $K_L^0 \rightarrow \pi^0 \pi^0 \pi^0$, $K_L^0 \rightarrow \pi^0 \pi^0$, signal and $2K_L^0$ decays clockwise from top left. All cuts prior to the cuts on this distribution are applied. The distributions are weighted.

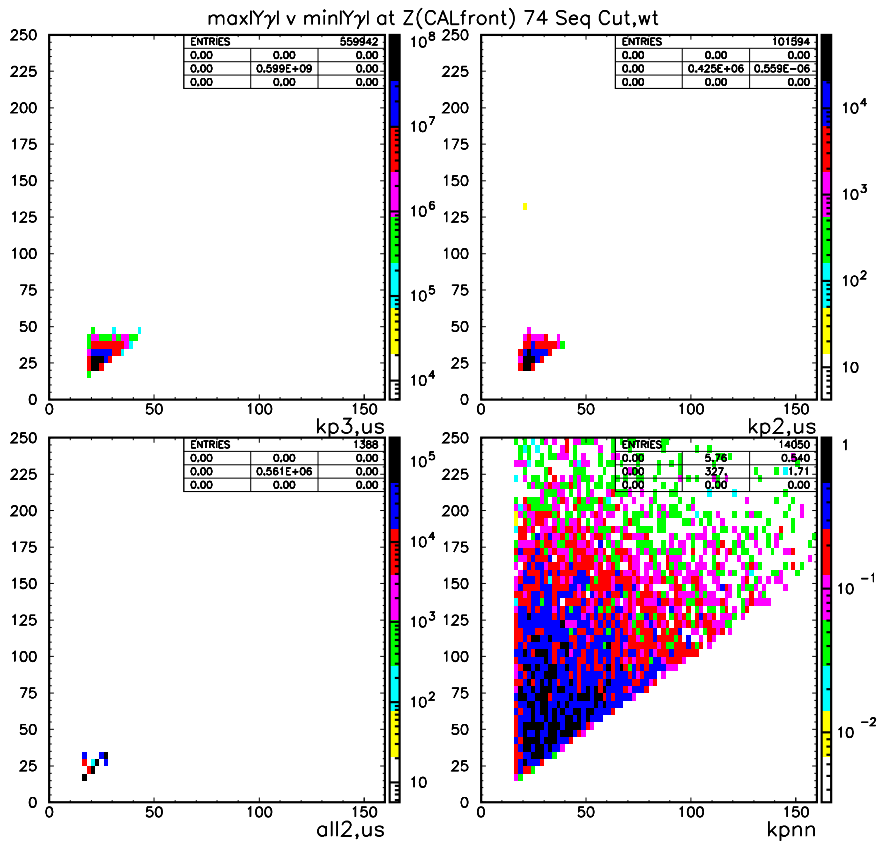
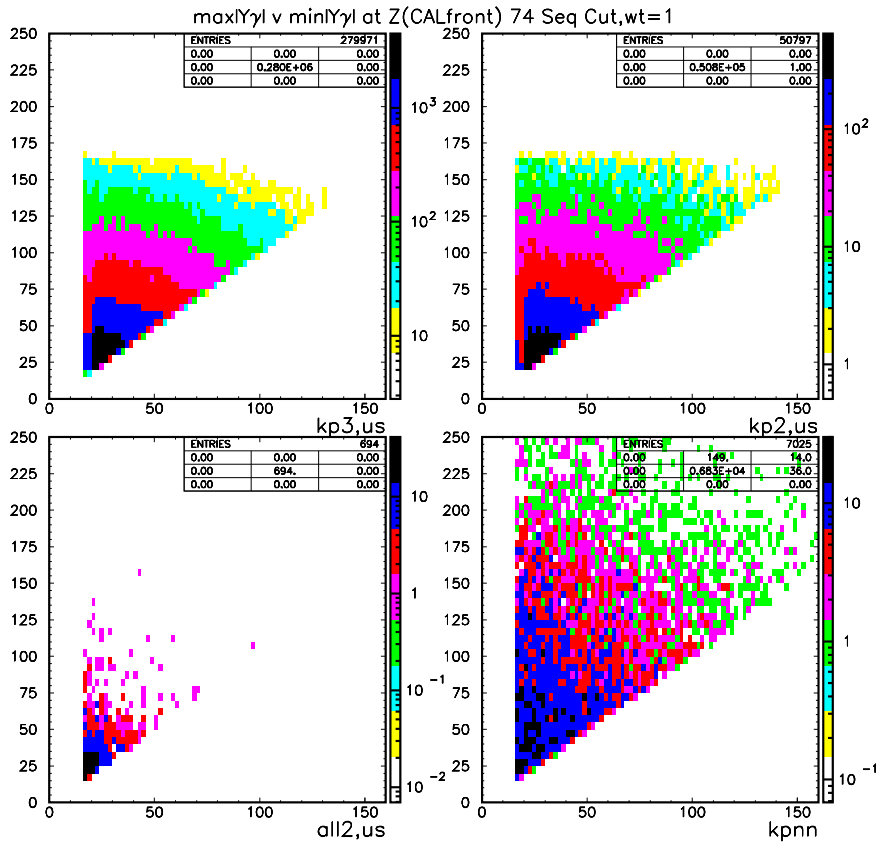


Figure 6: Distribution of $\max(|y_{\gamma 1}|, |y_{\gamma 2}|)$ vs $\min(|y_{\gamma 1}|, |y_{\gamma 2}|)$ for $K_L^0 \rightarrow \pi^0 \pi^0 \pi^0$, $K_L^0 \rightarrow \pi^0 \pi^0$, signal and $2K_L^0$ decays clockwise from top left. All cuts prior to the cuts on this distribution are applied. The distributions in the top (bottom) quartet are unweighted (weighted).

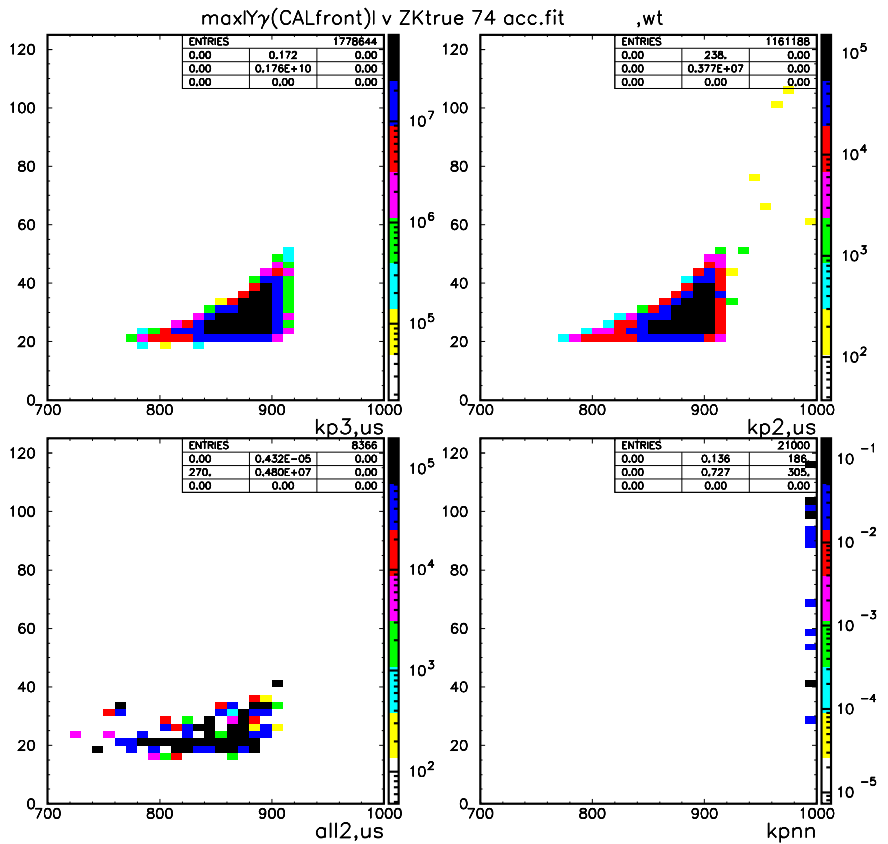
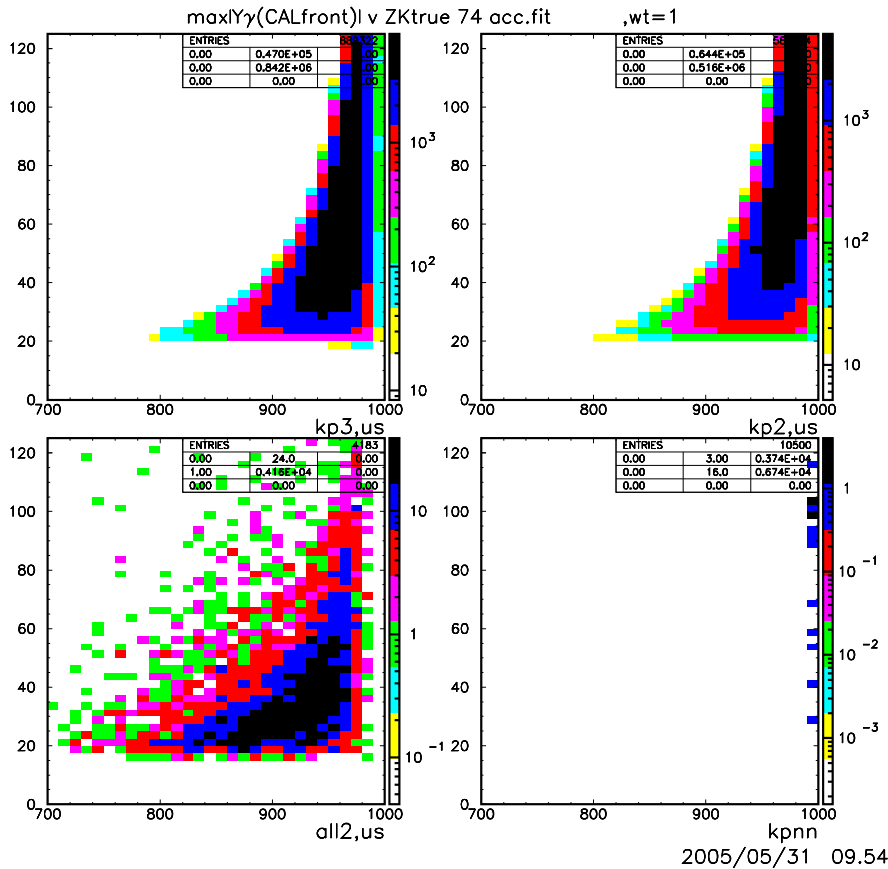


Figure 7: Distribution of $\max(|y_{\gamma 1}|, |y_{\gamma 2}|)$ vs the true z position of the K_L^0 decay for $K_L^0 \rightarrow \pi^0 \pi^0 \pi^0$, $K_L^0 \rightarrow \pi^0 \pi^0$, signal and $2K_L^0$ decays clockwise from top left. The “Geo-mAcc” and “GoodFit” cuts have been applied. The distributions in the top (bottom) quartet are unweighted (weighted).

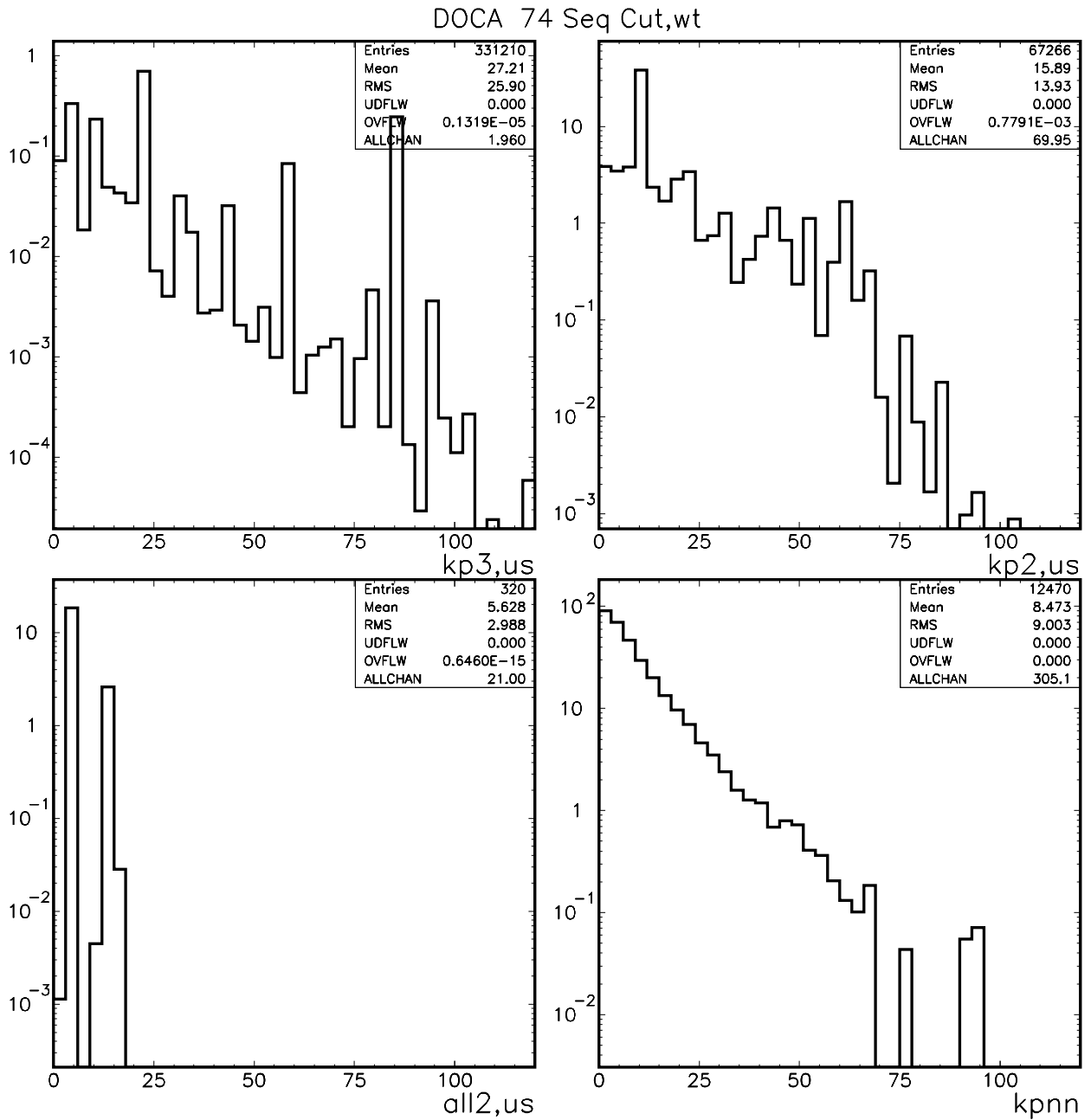


Figure 8: Distribution of DOCA for $K_L^0 \rightarrow \pi^0\pi^0\pi^0$, $K_L^0 \rightarrow \pi^0\pi^0$, signal and $2K_L^0$ decays clockwise from top left. All cuts prior to the cuts on this distribution are applied. The distributions are weighted.

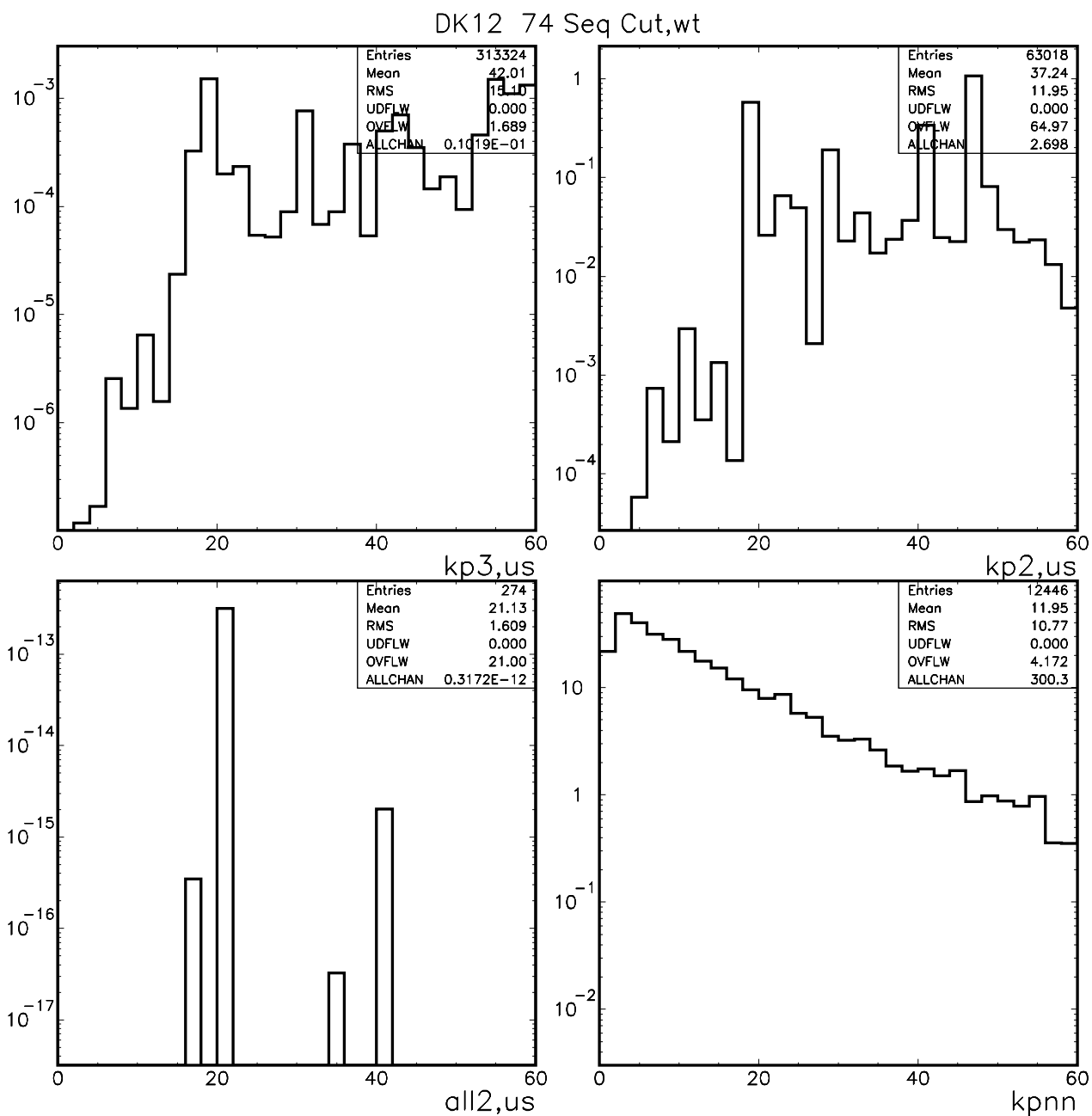


Figure 9: Distribution of DK12 for $K_L^0 \rightarrow \pi^0 \pi^0 \pi^0$, $K_L^0 \rightarrow \pi^0 \pi^0$, signal and $2K_L^0$ decays clockwise from top left. All cuts prior to the cuts on this distribution are applied. The distributions are weighted.

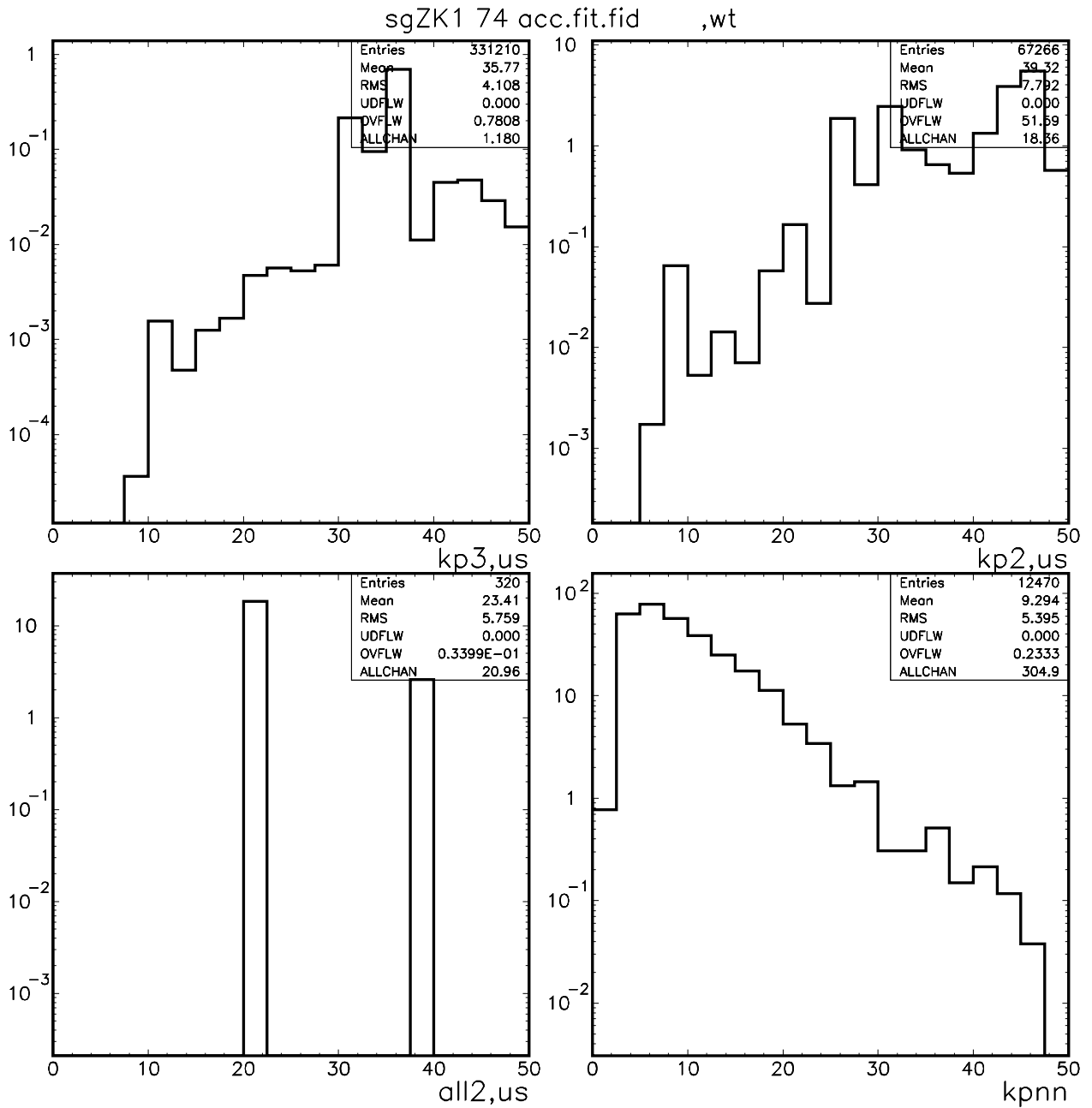


Figure 10: Distribution of sgZK1 for $K_L^0 \rightarrow \pi^0\pi^0\pi^0$, $K_L^0 \rightarrow \pi^0\pi^0$, signal and $2K_L^0$ decays clockwise from top left. The “GeomAcc”, “GoodFit” and “Fiducial” cuts have been applied. The distributions are weighted.

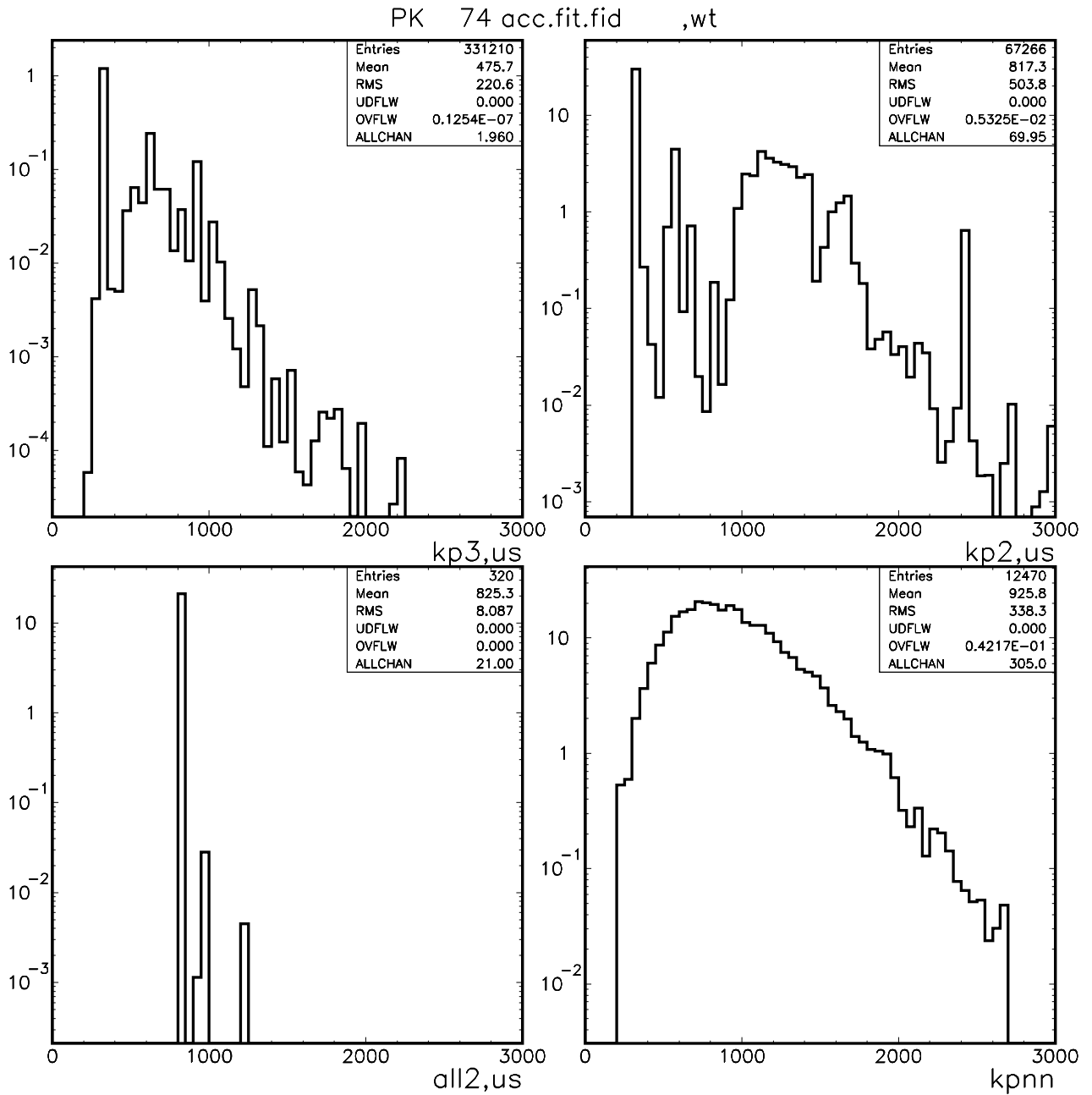


Figure 11: Distribution of PK for $K_L^0 \rightarrow \pi^0\pi^0\pi^0$, $K_L^0 \rightarrow \pi^0\pi^0$, signal and $2K_L^0$ decays clockwise from top left. The “GeomAcc”, “GoodFit” and “Fiducial” cuts have been applied. The distributions are weighted.

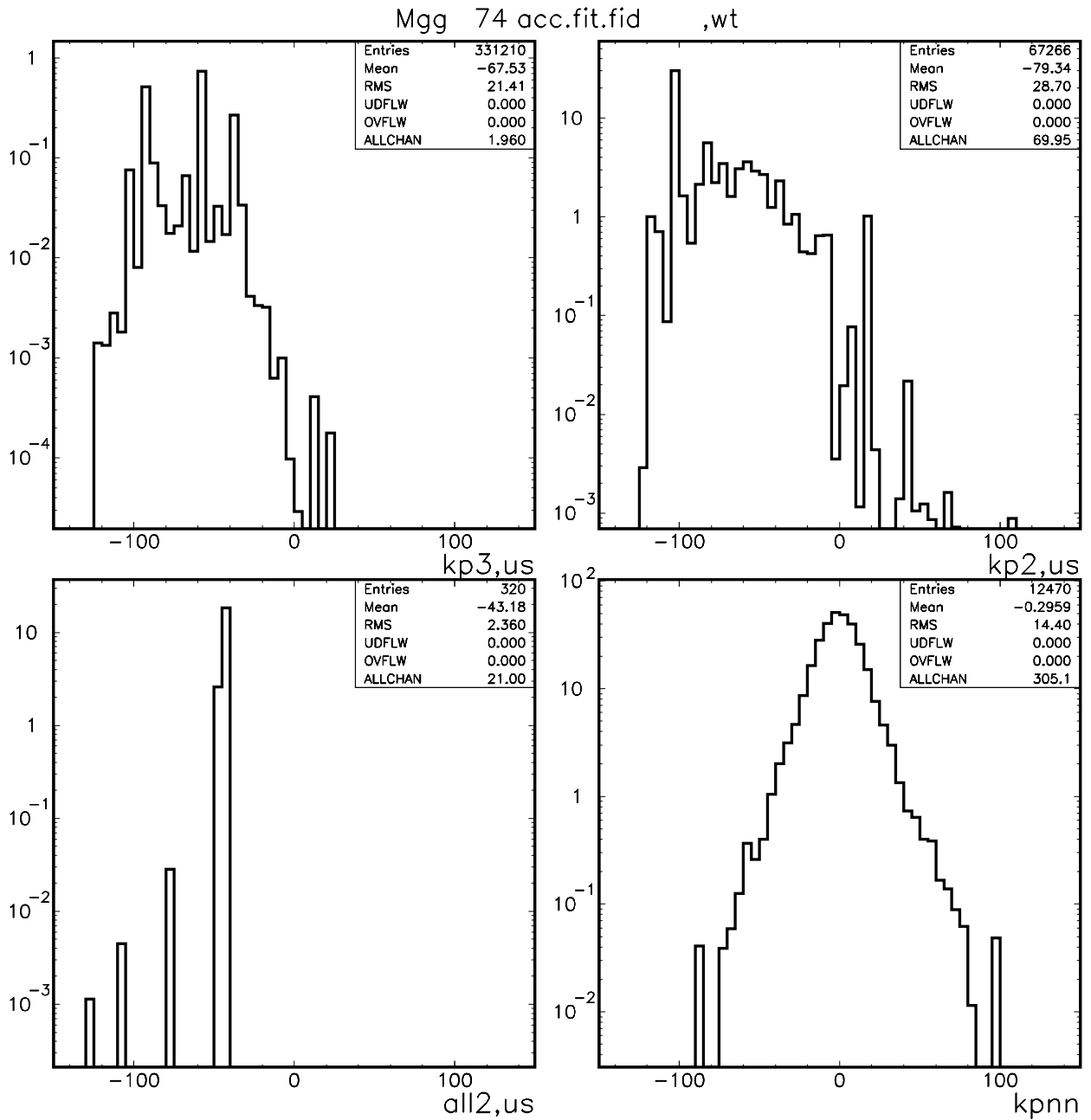


Figure 12: Distribution of $M(\gamma\gamma) - M(\pi^0)$ for $K_L^0 \rightarrow \pi^0\pi^0\pi^0$, $K_L^0 \rightarrow \pi^0\pi^0$, signal and $2K_L^0$ decays clockwise from top left. The “GeomAcc”, “GoodFit” and “Fiducial” cuts have been applied. The distributions are weighted.

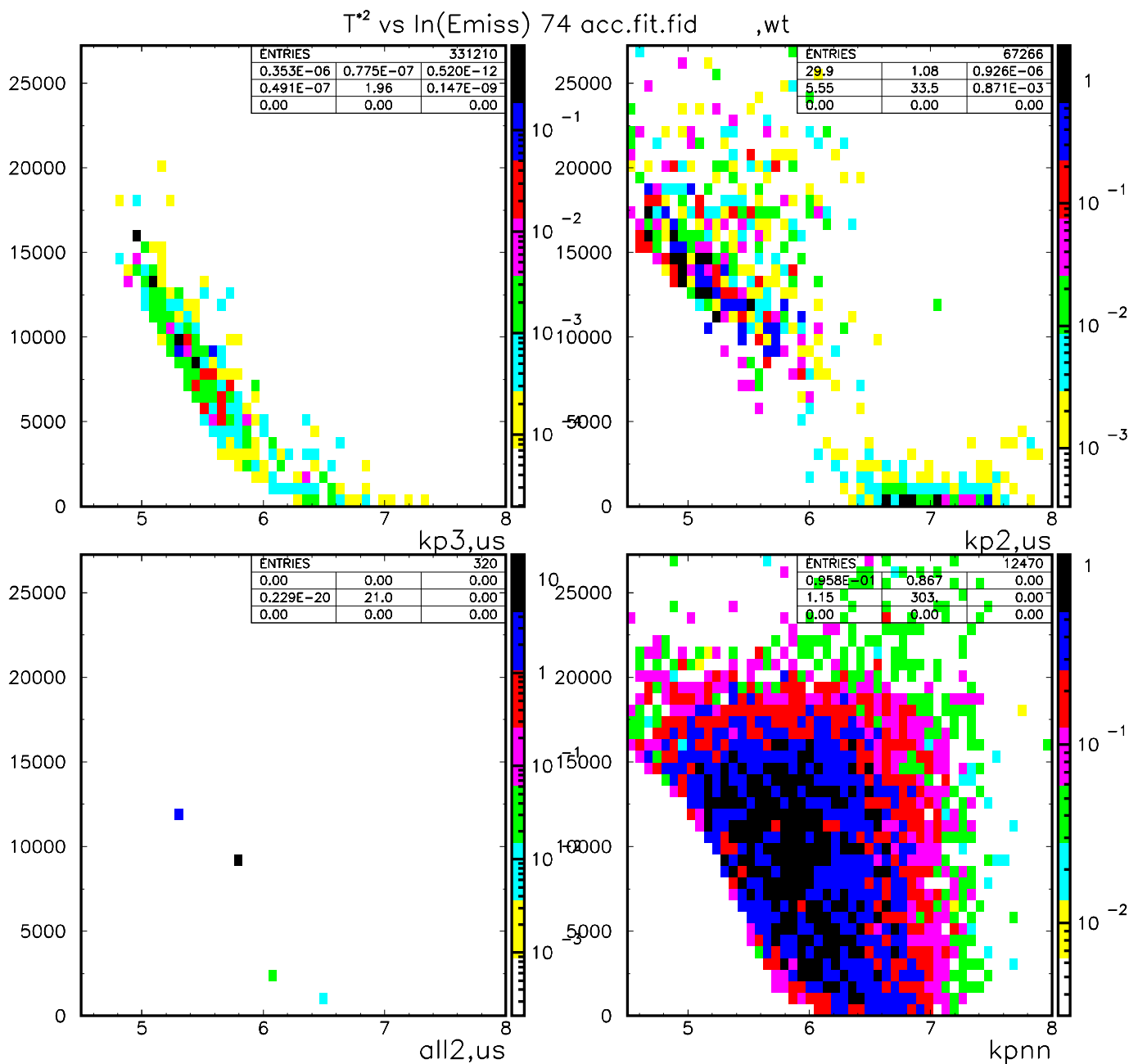


Figure 13: Distribution of $T^*{}^2$ vs $\ln(E_{\text{miss}})$ for $K_L^0 \rightarrow \pi^0\pi^0\pi^0$, $K_L^0 \rightarrow \pi^0\pi^0$, signal and $2K_L^0$ decays clockwise from top left. The “GeomAcc”, “GoodFit” and “Fiducial” cuts have been applied. The distributions are weighted.

4 Expected background rates

The expected background rates listed in this note assume a total of 1.27×10^{15} useful K_L^0 exiting the spoiler in a 12000 hour run. By “useful” I mean that losses due to accidentals, self-veto and photon absorption are taken into account. For the spill length optimization cited in the CDR, the the total number of useful K_L^0 exiting the spoiler was 0.57×10^{15} . If this optimization is correct, then the rates in this note need to be scaled by $0.449 = 0.57/1.27$. In addition, the rate for K_L^0 pairs does not take into account the probability that at least 2 K_L^0 exit the spoiler in a microbunch. (If the mean number of K_L^0 exiting the spoiler per microbunch is 2.0, then the probability of at least 2 K_L^0 is 59%.)

Tables 3, 4, 5 and 6 show the effectiveness of the cuts described in Section 3 and the expected background and signal rates.

Solid angle considerations reduce the Kp3 and Kp2 rates by 0.3% and 0.2%, respectively, as shown in Column 2 of Tables 3 and 4. The suppression for the K_L^0 pairs is much greater at 6.8×10^{-6} (Table 5).

One measure of background rejection of a cut is the efficiency to pass the cut when all previous cuts have been applied. Using this measure, it is clear from the 11th column (“Eff.seq”) in Table 3 that the **YatCL** provides the biggest background rejection factor for Kp3. This is also clear from Figure 7. A requirement on the minimum **YatCL** forces the K_L^0 decay point further downstream where the decay products can be efficiently vetoed. The “MisRecon” cuts (**DOCA**, **DK12**, **sgZK1**) provide an additional background suppression factor of 1.2×10^{-3} while other cuts provide only modest background suppression.

The **YatCL** cut also provides the biggest background rejection factor for Kp2 of 0.16×10^{-3} and the “MisRecon” cuts provide an additional background suppression factor of 0.43×10^{-3} . The most powerful single cut of the “MisRecon” cuts is **DK12** that takes advantage of the difference between the $z(K_L^0)$ of the first and second fits.

For the K_L^0 pairs, Table 5, the **YatCL** and **DK12** cuts provide the greatest suppression. Comparison of this table with that for single Kp3 or Kp2 decays shows that there is additional suppression from the **Chi2n** and **delt** cuts as expected.

The loss of signal due to the **YatCL** cut, that was not taken into account for the April 2005 Baseline, is 8.9%. A proposal to recover some of this lost acceptance is described in the next section. The **ZK** cut has a 70.6% efficiency due to the fact that signal decays are generated over the entire 400 cm decay volume but the fiducial volume is only 275 cm long.

5 Another veto in the upstream beam pipe

There is a clear correlation between the maximum photon impact position at the calorimeter and the z position of the K_L^0 decay as shown in Figure 7. With the assumptions in Section 2, there are two independent methods available to suppress backgrounds from US K_L^0 decays. One method is the cut on **YatCL** described earlier. The second would be to introduce another veto detector upstream of the UV.

Figure 14 shows the expected number of background events as a function of the true z of $K_L^0 \rightarrow \pi^0\pi^0\pi^0$ decays. The UV extends to $z = 917$ cm and, from Figure 14, K_L^0 decays to $z > 900$ cm are sufficiently suppressed. From this observation, I assume that any additional veto will be able to suppress K_L^0 decays ~ 20 cm upstream of the veto’s most upstream point. With this assumption, an additional veto (call it the “WV” for Way upstream Veto) that occupied the region $860 < z < 917$ ($820 < z < 917$) cm would suppress the Kp3 background by an additional factor of ~ 10 (~ 100) assuming that the WV had the same or better veto efficiency as the UV.

If K_L^0 decays dominate the accidental veto losses from such a detector, then the accidental loss rate would probably be acceptable. A relatively narrow veto timing

Unweighted							Expected numbers of events							Cut
N(pass)	Eff.1st	N(pass)	Eff.seq	Nbefore	Nafter	Eff.last	N(pass)	Eff.1st	N(pass)	Eff.seq	Nbefore	Nafter	Eff.last	
0.300E+09	0.00	0.300E+09	0.00	0.300E+09	0.300E+09	0.00	0.267E+15	0.00	0.267E+15	0.00	0.267E+15	0.267E+15	0.00	NONE
0.925E+06	0.308E-02	0.925E+06	0.308E-02	736.	736.	1.00	0.189E+10	0.706E-05	0.189E+10	0.706E-05	0.356E-03	0.356E-03	1.00	Accpt
0.158E+07	0.528E-02	0.902E+06	0.975	736.	736.	1.00	0.219E+10	0.820E-05	0.180E+10	0.956	0.356E-03	0.356E-03	1.00	Ierr
0.157E+07	0.523E-02	0.893E+06	0.990	736.	736.	1.00	0.216E+10	0.806E-05	0.177E+10	0.982	0.356E-03	0.356E-03	1.00	ValKL
0.160E+07	0.532E-02	0.889E+06	0.996	736.	736.	1.00	0.220E+10	0.824E-05	0.176E+10	0.994	0.356E-03	0.356E-03	1.00	Chi2n
0.162E+07	0.539E-02	0.888E+06	0.998	743.	736.	0.991	0.229E+10	0.855E-05	0.176E+10	0.999	0.356E-03	0.356E-03	1.000	delT
0.152E+07	0.508E-02	0.864E+06	0.974	740.	736.	0.995	0.208E+10	0.779E-05	0.166E+10	0.945	0.356E-03	0.356E-03	1.000	XK
0.871E+06	0.290E-02	0.438E+06	0.507	908.	736.	0.811	0.112E+10	0.419E-05	0.843E+09	0.507	0.412E-03	0.356E-03	0.864	Yk
0.104E+07	0.347E-02	0.280E+06	0.639	0.804E+04	736.	0.915E-01	0.145E+10	0.542E-05	0.599E+09	0.710	0.219E-02	0.356E-03	0.163	ZK
0.899E+06	0.300E-02	0.166E+06	0.592	0.112E+04	736.	0.657	0.250E+06	0.934E-09	1.96	0.327E-08	0.302E+06	0.356E-03	0.118E-08	YatCL
0.156E+07	0.519E-02	0.157E+06	0.946	736.	736.	1.00	0.218E+10	0.815E-05	1.70	0.867	0.356E-03	0.356E-03	1.00	DOCA
0.114E+06	0.380E-03	0.181E+04	0.116E-01	0.238E+04	736.	0.309	0.773E+08	0.289E-06	0.251E-02	0.147E-02	0.173E-02	0.356E-03	0.206	DK12
0.282E+06	0.939E-03	0.173E+04	0.954	760.	736.	0.968	0.220E+09	0.823E-06	0.228E-02	0.911	0.356E-03	0.356E-03	1.000	sgZK1
0.160E+07	0.533E-02	0.173E+04	1.00	736.	736.	1.00	0.224E+10	0.838E-05	0.228E-02	1.00	0.356E-03	0.356E-03	1.00	PK
0.162E+07	0.540E-02	0.173E+04	1.00	736.	736.	1.00	0.228E+10	0.854E-05	0.228E-02	1.00	0.356E-03	0.356E-03	1.00	Eg
0.128E+07	0.426E-02	0.130E+04	0.751	784.	736.	0.939	0.151E+10	0.564E-05	0.187E-02	0.819	0.389E-03	0.356E-03	0.916	Mnu2
0.363E+06	0.121E-02	0.130E+04	0.999	736.	736.	1.00	0.264E+09	0.987E-06	0.187E-02	1.000	0.356E-03	0.356E-03	1.00	Mgg
0.159E+07	0.529E-02	0.130E+04	1.00	736.	736.	1.00	0.229E+10	0.855E-05	0.187E-02	1.00	0.356E-03	0.356E-03	1.00	E*pi
0.167E+06	0.557E-03	736.	0.568	0.130E+04	736.	0.568	0.109E+09	0.408E-06	0.356E-03	0.190	0.187E-02	0.356E-03	0.190	Like

Table 3: Cut survival table for $K_L^0 \rightarrow \pi^0 \pi^0 \pi^0$ decays upstream of the decay region. The seven columns on the left are unweighted events. The next seven columns are weighted by decay probability, K_L^0 production rate, conversion probability and veto inefficiency to produce the expected number of events for the full running period of KOPIO. The fifteenth column lists the five letter acronym of the applied cuts defined in Section 3. The top row (Cut “NONE”) gives the total number of simulated K_L^0 decays. The first column is the number of events that pass the cut. The second column is the efficiency of the cut when it is applied first, before all other cuts. The third column is the number of events passing the cuts listed in the sequence in the fifteenth column. The fourth column is the efficiency of the cut when applied in sequence. The fifth column is the number of events passing all other cuts except the cut in that row. The sixth column is the number of events passing all cuts. The seventh column is the efficiency of the cut when applied last, after all other cuts. Columns eight through fourteen are similar.

Unweighted							Expected numbers of events							Cut
N(pass)	Eff.1st	N(pass)	Eff.seq	Nbefore	Nafter	Eff.last	N(pass)	Eff.1st	N(pass)	Eff.seq	Nbefore	Nafter	Eff.last	
0.300E+09	0.00	0.300E+09	0.00	0.300E+09	0.300E+09	0.00	0.118E+13	0.00	0.118E+13	0.00	0.118E+13	0.118E+13	0.00	NONE
0.592E+06	0.197E-02	0.592E+06	0.197E-02	143.	143.	1.00	0.392E+07	0.331E-05	0.392E+07	0.331E-05	0.311E-02	0.311E-02	1.00	Acpt
0.938E+06	0.313E-02	0.586E+06	0.990	143.	143.	1.00	0.477E+07	0.403E-05	0.383E+07	0.977	0.311E-02	0.311E-02	1.00	Ierr
0.935E+06	0.312E-02	0.584E+06	0.997	143.	143.	1.00	0.475E+07	0.401E-05	0.381E+07	0.994	0.311E-02	0.311E-02	1.00	ValKL
0.938E+06	0.313E-02	0.581E+06	0.994	143.	143.	1.00	0.476E+07	0.402E-05	0.377E+07	0.989	0.311E-02	0.311E-02	1.00	Chi2n
0.945E+06	0.315E-02	0.580E+06	0.998	143.	143.	1.00	0.485E+07	0.410E-05	0.376E+07	0.997	0.311E-02	0.311E-02	1.00	delT
0.928E+06	0.309E-02	0.574E+06	0.990	144.	143.	0.993	0.468E+07	0.395E-05	0.365E+07	0.972	0.336E-02	0.311E-02	0.928	XK
0.608E+06	0.203E-02	0.373E+06	0.649	171.	143.	0.836	0.266E+07	0.224E-05	0.206E+07	0.563	0.323E-02	0.311E-02	0.965	Yk
0.215E+06	0.716E-03	0.508E+05	0.136	0.481E+05	143.	0.297E-02	0.118E+07	0.997E-06	0.425E+06	0.207	3.60	0.311E-02	0.864E-03	ZK
0.697E+06	0.232E-02	0.336E+05	0.662	178.	143.	0.803	0.726E+04	0.613E-08	69.9	0.164E-03	0.386E-02	0.311E-02	0.807	YatCL
0.915E+06	0.305E-02	0.315E+05	0.937	143.	143.	1.00	0.465E+07	0.393E-05	67.7	0.967	0.311E-02	0.311E-02	1.00	DOCA
0.341E+06	0.111E-02	409.	0.130E-01	449.	143.	0.318	0.142E+07	0.120E-05	0.918	0.136E-01	0.259E-01	0.311E-02	0.120	DK12
0.429E+06	0.143E-02	292.	0.714	237.	143.	0.603	0.824E+06	0.695E-06	0.302E-01	0.328E-01	0.295E-01	0.311E-02	0.105	sgZK1
0.943E+06	0.311E-02	292.	1.00	143.	143.	1.00	0.483E+07	0.407E-05	0.302E-01	1.00	0.311E-02	0.311E-02	1.00	PK
0.945E+06	0.315E-02	291.	0.997	143.	143.	1.00	0.484E+07	0.408E-05	0.301E-01	1.000	0.311E-02	0.311E-02	1.00	Eg
0.539E+06	0.180E-02	246.	0.845	149.	143.	0.960	0.214E+07	0.181E-05	0.198E-01	0.657	0.319E-02	0.311E-02	0.977	Mnu2
0.599E+06	0.200E-02	245.	0.996	143.	143.	1.00	0.290E+07	0.245E-05	0.198E-01	0.999	0.311E-02	0.311E-02	1.00	Mgg
0.927E+06	0.309E-02	243.	0.992	143.	143.	1.00	0.481E+07	0.406E-05	0.312E-02	0.158	0.311E-02	0.311E-02	1.00	E*pi
0.277E+06	0.922E-03	143.	0.588	243.	143.	0.588	0.856E+06	0.722E-06	0.311E-02	0.997	0.312E-02	0.311E-02	0.997	Like

Table 4: Cut survival table for $K_L^0 \rightarrow \pi^0 \pi^0$ decays upstream of the decay region. The seven columns on the left are unweighted events. The next seven columns are weighted by decay probability, K_L^0 production rate, conversion probability and veto inefficiency to produce the expected number of events for the full running period of KOPIO. The fifteenth column lists the five letter acronym of the applied cuts defined in Section 3. The top row (Cut “NONE”) gives the total number of simulated K_L^0 decays. The first column is the number of events that pass the cut. The second column is the efficiency of the cut when it is applied first, before all other cuts. The third column is the number of events passing the cuts listed in the sequence in the fifteenth column. The fourth column is the efficiency of the cut when applied in sequence. The fifth column is the number of events passing all other cuts except the cut in that row. The sixth column is the number of events passing all cuts. The seventh column is the efficiency of the cut when applied last, after all other cuts. Columns eight through fourteen are similar.

Unweighted							Expected numbers of events							Cut
N(pass)	Eff.1st	N(pass)	Eff.seq	Nbefore	Nafter	Eff.last	N(pass)	Eff.1st	N(pass)	Eff.seq	Nbefore	Nafter	Eff.last	
0.140E+10	0.00	0.140E+10	0.00	0.140E+10	0.140E+10	0.00	0.127E+16	0.00	0.127E+16	0.00	0.127E+16	0.127E+16	0.00	NONE
0.947E+04	0.676E-05	0.947E+04	0.676E-05	1.00	1.00	1.00	0.115E+08	0.904E-08	0.115E+08	0.904E-08	0.315E-12	0.315E-12	1.00	Acpt
0.303E+06	0.21E-03	0.912E+04	0.963	1.00	1.00	1.00	0.714E+09	0.562E-06	0.109E+08	0.952	0.315E-12	0.315E-12	1.00	Terr
0.293E+06	0.209E-03	0.889E+04	0.975	1.00	1.00	1.00	0.642E+09	0.505E-06	0.106E+08	0.972	0.315E-12	0.315E-12	1.00	ValKL
0.174E+06	0.12E-03	0.418E+04	0.471	1.00	1.00	1.00	0.407E+09	0.320E-06	0.480E+07	0.452	0.315E-12	0.315E-12	1.00	Chi2n
0.858E+05	0.613E-04	0.184E+04	0.440	1.00	1.00	1.00	0.205E+09	0.162E-06	0.144E+07	0.300	0.315E-12	0.315E-12	1.00	delT
0.270E+06	0.193E-03	0.179E+04	0.971	1.00	1.00	1.00	0.734E+09	0.578E-06	0.138E+07	0.961	0.315E-12	0.315E-12	1.00	XK
0.214E+06	0.153E-03	990.	0.554	1.00	1.00	1.00	0.609E+09	0.479E-06	0.876E+06	0.633	0.315E-12	0.315E-12	1.00	Yk
0.141E+06	0.101E-03	694.	0.701	3.00	1.00	0.333	0.459E+09	0.361E-06	0.561E+06	0.641	0.315E-12	0.315E-12	1.00	ZK
0.327E+05	0.23E-04	160.	0.231	1.00	1.00	1.00	0.841E+04	0.661E-11	21.0	0.374E-04	0.315E-12	0.315E-12	1.00	YatCL
0.308E+06	0.220E-03	137.	0.856	1.00	1.00	1.00	0.710E+09	0.558E-06	21.0	1.00	0.315E-12	0.315E-12	1.00	DOCA
0.130E+05	0.931E-05	3.00	0.219E-01	4.00	1.00	0.250	0.110E+08	0.864E-08	0.315E-12	0.150E-13	0.31E-12	0.315E-12	0.993	DK12
0.107E+06	0.766E-04	3.00	1.00	1.00	1.00	1.00	0.169E+09	0.133E-06	0.315E-12	1.00	0.315E-12	0.315E-12	1.00	sgZK1
0.321E+06	0.230E-03	3.00	1.00	1.00	1.00	1.00	0.686E+09	0.540E-06	0.315E-12	1.00	0.315E-12	0.315E-12	1.00	PK
0.322E+06	0.230E-03	3.00	1.00	1.00	1.00	1.00	0.761E+09	0.599E-06	0.315E-12	1.00	0.315E-12	0.315E-12	1.00	Eg
0.216E+06	0.15E-03	3.00	1.00	1.00	1.00	1.00	0.522E+09	0.411E-06	0.315E-12	1.00	0.315E-12	0.315E-12	1.00	Mnu2
0.670E+05	0.478E-04	3.00	1.00	1.00	1.00	1.00	0.232E+08	0.183E-07	0.315E-12	1.00	0.315E-12	0.315E-12	1.00	Mgg
0.328E+06	0.23E-03	3.00	1.00	1.00	1.00	1.00	0.756E+09	0.595E-06	0.315E-12	1.00	0.315E-12	0.315E-12	1.00	E*pi
0.234E+05	0.16E-04	1.00	0.333	3.00	1.00	0.333	0.634E+07	0.499E-08	0.315E-12	0.999	0.315E-12	0.315E-12	0.999	Like

Table 5: Cut survival table for 2 K_L^0 decays upstream of the decay region. The seven columns on the left are unweighted events. The next seven columns are weighted by decay probability, K_L^0 production rate, conversion probability and veto inefficiency to produce the expected number of events for the full running period of KOPIO. The fifteenth column lists the five letter acronym of the applied cuts defined in Section 3. The top row (Cut “NONE”) gives the total number of simulated K_L^0 decays. The first column is the number of events that pass the cut. The second column is the efficiency of the cut when it is applied first, before all other cuts. The third column is the number of events passing the cuts listed in the sequence in the fifteenth column. The fourth column is the efficiency of the cut when applied in sequence. The fifth column is the number of events passing all other cuts except the cut in that row. The sixth column is the number of events passing all cuts. The seventh column is the efficiency of the cut when applied last, after all other cuts. Columns eight through fourteen are similar.

Unweighted							Expected numbers of events							Cut
N(pass)	Eff.1st	N(pass)	Eff.seq	Nbefore	Nafter	Eff.last	N(pass)	Eff.1st	N(pass)	Eff.seq	Nbefore	Nafter	Eff.last	
0.500E+05	0.00	0.500E+05	0.00	0.500E+05	0.500E+05	0.00	0.381E+05	0.00	0.381E+05	0.00	0.381E+05	0.381E+05	0.00	NONE
0.105E+05	0.210	0.105E+05	0.210	0.382E+04	0.382E+04	1.00	493.	0.129E-01	493.	0.129E-01	176.	176.	1.00	Accept
0.471E+05	0.943	0.105E+05	1.00	0.382E+04	0.382E+04	1.00	640.	0.168E-01	493.	1.00	176.	176.	1.00	Terr
0.471E+05	0.943	0.105E+05	1.00	0.382E+04	0.382E+04	1.00	640.	0.168E-01	493.	1.00	176.	176.	1.00	ValKL
0.471E+05	0.942	0.105E+05	0.999	0.382E+04	0.382E+04	0.999	639.	0.168E-01	492.	0.999	176.	176.	1.000	Chi2n
0.471E+05	0.942	0.105E+05	0.999	0.382E+04	0.382E+04	0.999	639.	0.168E-01	492.	0.999	176.	176.	0.999	delT
0.468E+05	0.937	0.104E+05	0.990	0.384E+04	0.382E+04	0.996	633.	0.166E-01	487.	0.989	177.	176.	0.995	XK
0.457E+05	0.914	0.101E+05	0.974	0.386E+04	0.382E+04	0.990	622.	0.163E-01	474.	0.975	178.	176.	0.992	Yk
0.329E+05	0.659	0.702E+04	0.695	0.545E+04	0.382E+04	0.701	456.	0.120E-01	335.	0.706	253.	176.	0.696	ZK
0.434E+05	0.868	0.624E+04	0.888	0.425E+04	0.382E+04	0.898	578.	0.152E-01	305.	0.911	191.	176.	0.921	YatCL
0.463E+05	0.927	0.622E+04	0.998	0.382E+04	0.382E+04	1.00	637.	0.167E-01	305.	0.998	176.	176.	1.00	DOCA
0.395E+05	0.790	0.567E+04	0.911	0.403E+04	0.382E+04	0.948	567.	0.149E-01	278.	0.912	186.	176.	0.948	DK12
0.462E+05	0.924	0.564E+04	0.996	0.383E+04	0.382E+04	0.997	615.	0.161E-01	277.	0.996	177.	176.	0.997	sgZK1
0.450E+05	0.901	0.555E+04	0.983	0.384E+04	0.382E+04	0.995	624.	0.164E-01	271.	0.978	177.	176.	0.994	PK
0.410E+05	0.820	0.537E+04	0.968	0.396E+04	0.382E+04	0.963	611.	0.160E-01	262.	0.968	183.	176.	0.962	Eg
0.385E+05	0.770	0.414E+04	0.771	0.397E+04	0.382E+04	0.962	461.	0.121E-01	191.	0.729	184.	176.	0.955	Mnu2
0.459E+05	0.918	0.409E+04	0.988	0.382E+04	0.382E+04	1.00	615.	0.161E-01	189.	0.988	176.	176.	1.00	Mgg
0.471E+05	0.941	0.408E+04	0.996	0.382E+04	0.382E+04	1.00	637.	0.167E-01	188.	0.997	176.	176.	1.00	E*pi
0.357E+05	0.713	0.382E+04	0.937	0.408E+04	0.382E+04	0.937	432.	0.113E-01	176.	0.936	188.	176.	0.936	Like

Table 6: Cut survival table for signal decays in the decay region. The seven columns on the left are unweighted events. The next seven columns are weighted by decay probability, K_L^0 production rate, conversion probability and veto inefficiency to produce the expected number of events for the full running period of KOPIO. The fifteenth column lists the five letter acronym of the applied cuts defined in Section 3. The top row (Cut “NONE”) gives the total number of simulated K_L^0 decays. The first column is the number of events that pass the cut. The second column is the efficiency of the cut when it is applied first, before all other cuts. The third column is the number of events passing the cuts listed in the sequence in the fifteenth column. The fourth column is the efficiency of the cut when applied in sequence. The fifth column is the number of events passing all other cuts except the cut in that row. The sixth column is the number of events passing all cuts. The seventh column is the efficiency of the cut when applied last, after all other cuts. Columns eight through fourteen are similar.

window would be possible for the WV because we could compare the extrapolated time of the photons detected in the PR/CAL with the WV hit times. Losses could also be reduced because we would only need to use the veto for events with $\text{YatCL} < 50$ cm.

If the WV provided sufficient suppression by itself, then the YatCL cut could be relaxed and some of the $\sim 9\%$ of signal acceptance that was lost to the YatCL cut could be regained.

Precise design of the WV is probably requires a more detailed simulation (GEANT4).

6 Effect of the size of the US hole

The aperture of the beam pipe as it enters the decay region defines the acceptance for photons from US K_L^0 decays. Figure 15 shows the maximum vertical displacement (Yuhol) of the two photon candidates at this point. Within the limited statistical precision available, it appears that the Kp3 and Kp2 background rates are approximately constant for $\text{Yuhol} >$ a few cm. This would imply that there would be no huge increase in background due to photons that traverse a portion of the beam pipe that defines the aperture. Similarly, decreasing the aperture would not lead to a massive decrease in this background.

7 An alternative to the YatCL cut?

Laur suggested that photons from US K_L^0 that lead to mis-reconstructed candidates might preferentially be above or below the beam. Figure 16 shows that there is indeed a disparity between the signal and the background distributions for $\text{sYmax} \equiv \text{sign}(\max(|y_{\gamma_1}|, |y_{\gamma_2}|), y_{\gamma_1} \times y_{\gamma_2})$ position of the photon candidates at the z of the front of the calorimeter. Since the steep drop in the background occurs at the same point for sYmax greater and less than zero, simple cuts on this variable would not be more effective than the YatCL cut.

8 Other distributions

In this section some other distributions of background and signal are plotted and discussed. Although none of these distributions appear to me to be better than YatCL at suppressing the US background, it may be possible to take correlations between the distributions into account and get comparable background rejection with less signal loss. I have not investigated this possibility.

Figure 17 shows the energy of the photon with the maximum absolute y position extrapolated to the front of the calorimeter vs maximum absolute y position. This is essentially the energy of the photon that defines YatCL . There does not appear to be much to be gained from a cut on the energy because the distribution for Kp3 is similar to that for signal.

The distributions of the measured opening angle between the detected photons is shown in Figure 18. Geometric considerations obviously force the opening angle of the US photons to be smaller on average than that for signal, but a cut on YatCL still has better signal acceptance for comparable background rejection than a cut on the opening angle.

The distributions of the energy asymmetry $\mathcal{A} \equiv |E_1 - E_2|/(E_1 + E_2)$ is shown in Figure 19. The Kp3 and Kp2 distributions differ from signal and Kp2 is dominated by Kp2-odd with asymmetric pairs. The shape of the Kp3 and signal distributions are both flat in the large region of overlap, so there does not appear to be any possibility to cut on these distributions. The region of the \mathcal{A} that is populated by signal ($\mathcal{A} > .9$) but not by background may indicate a region with high signal-to-background; however, the same distributions need to be examined for the other sources of background.

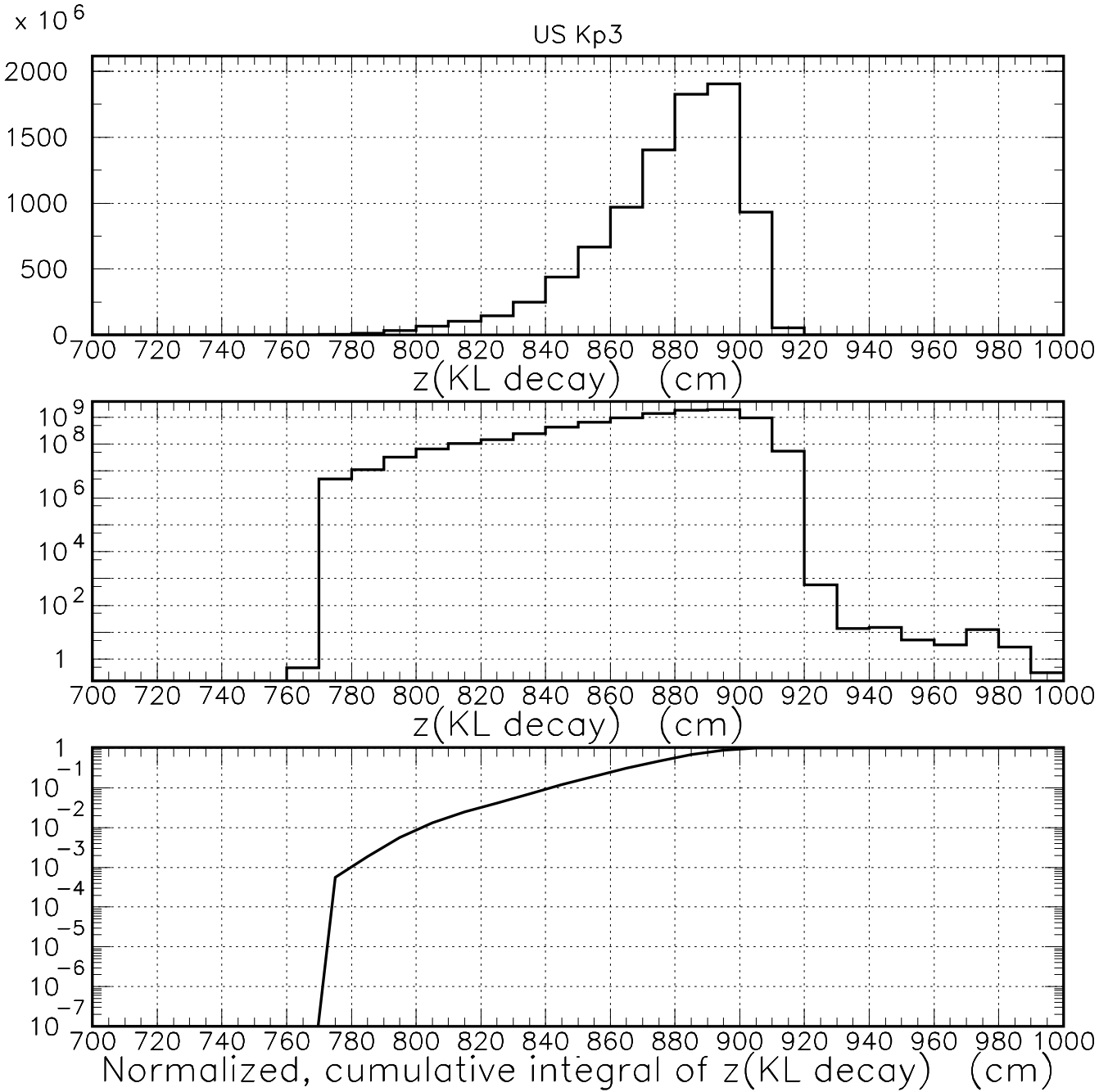


Figure 14: The expected number of background events as a function of the true z position of the K_L^0 decay for US $K_L^0 \rightarrow \pi^0\pi^0\pi^0$ decays that pass the “GeomAcc” and “GoodFit” cuts.

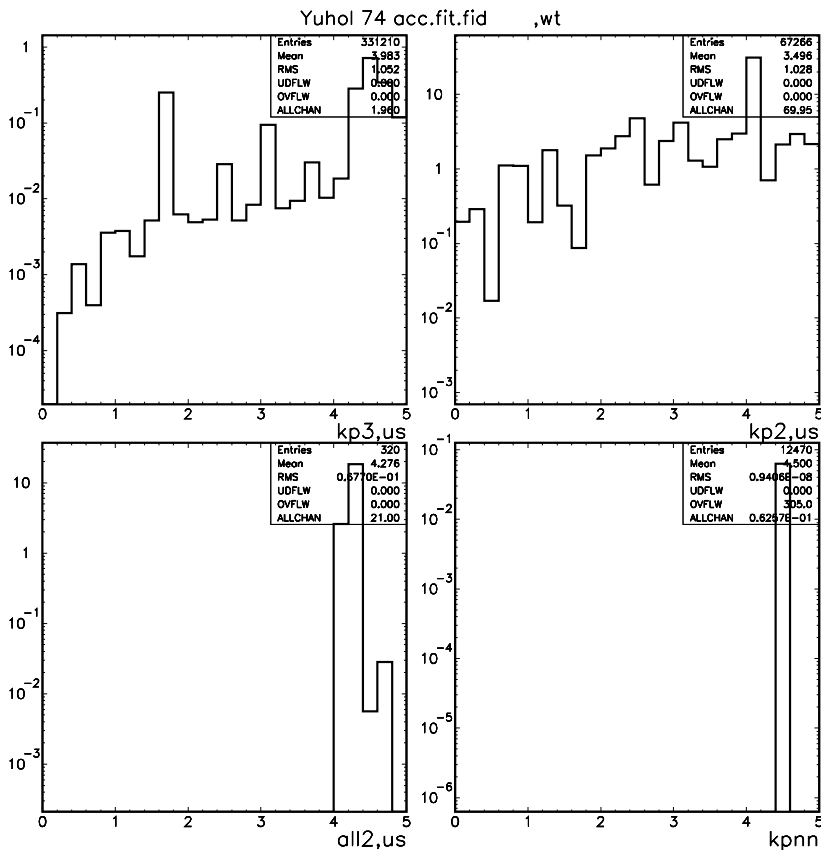
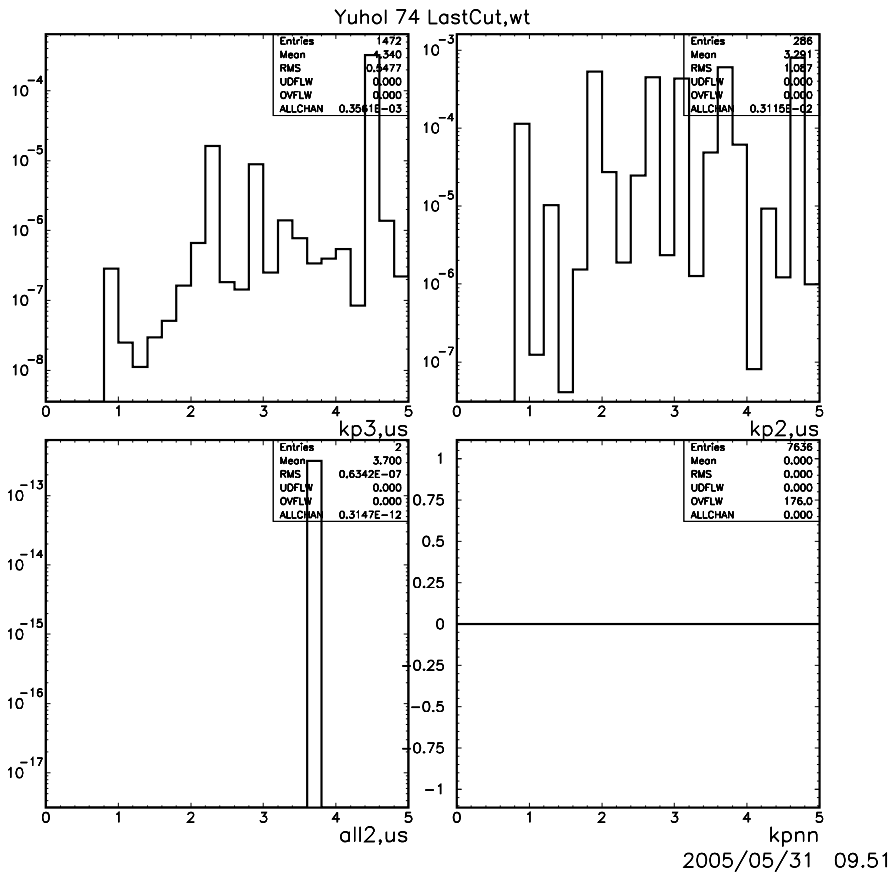


Figure 15: The expected number of background events as a function of the extrapolated true $\max(|y_{\gamma 1}|, |y_{\gamma 2}|)$ position of the photon candidates at the exit of the US beam pipe ($z = 997$ cm). Top quartet: after all cuts. Bottom quartet: after the “GeomAcc”, “GoodFit” and “Fiducial” cuts.

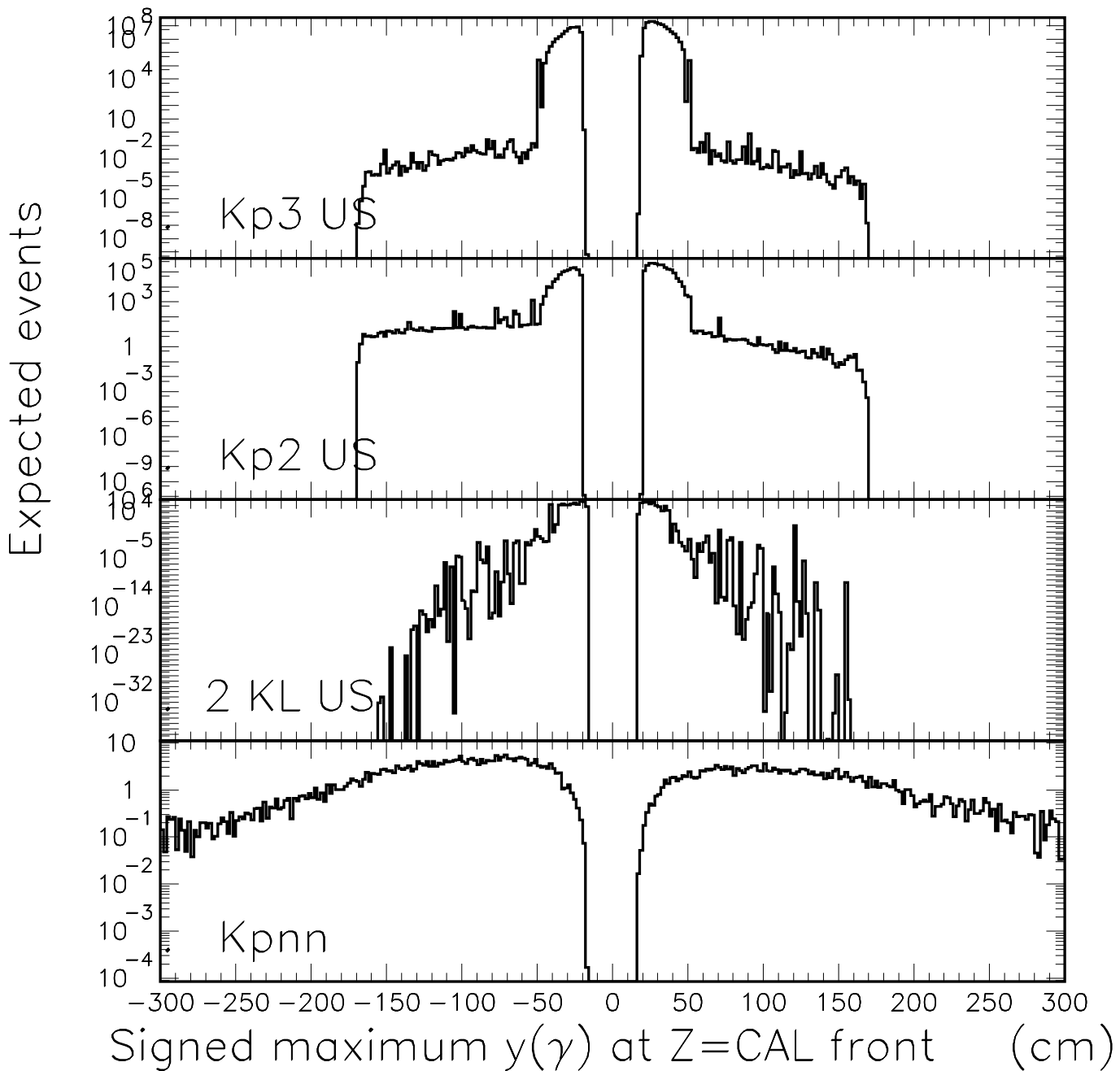


Figure 16: The expected number of background events as a function of the signed, extrapolated true $sY_{max} \equiv \text{sign}(\max(|y_{\gamma 1}|, |y_{\gamma 2}|), y_{\gamma 1} \times y_{\gamma 2})$ position of the photon candidates at the z of the front of the calorimeter after the “GeomAcc”, “GoodFit” and “Fiducial” cuts. Positive values of sY_{max} correspond to the case where both photons are either above or below $y = 0$. Negative values of sY_{max} correspond to the case where the photons are above and below the beam.

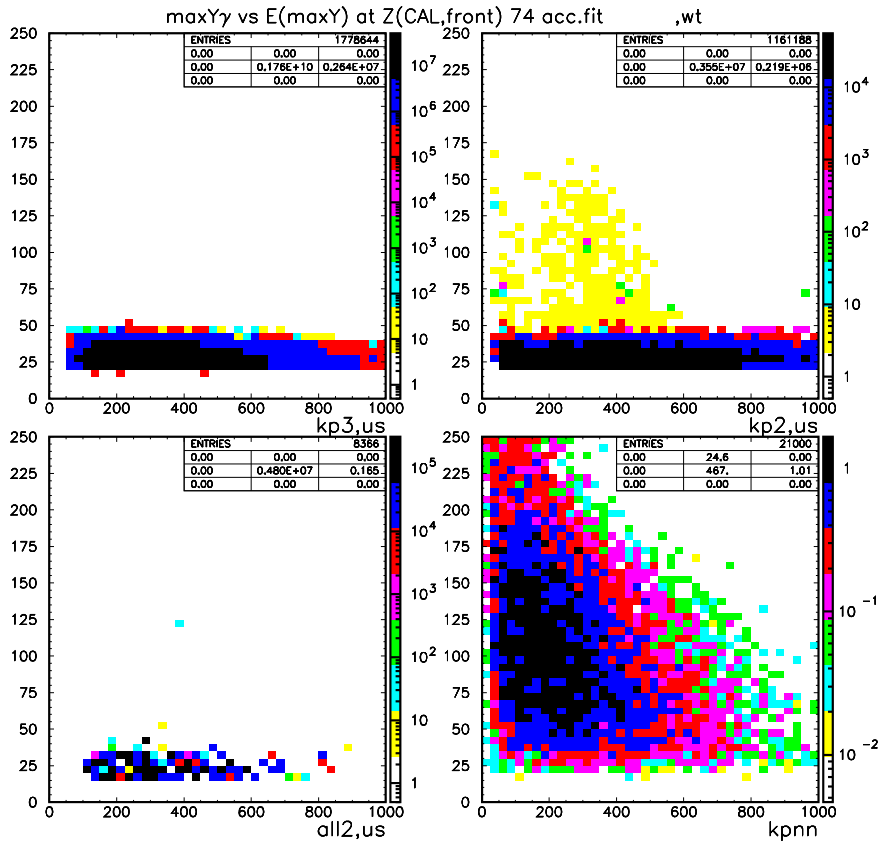
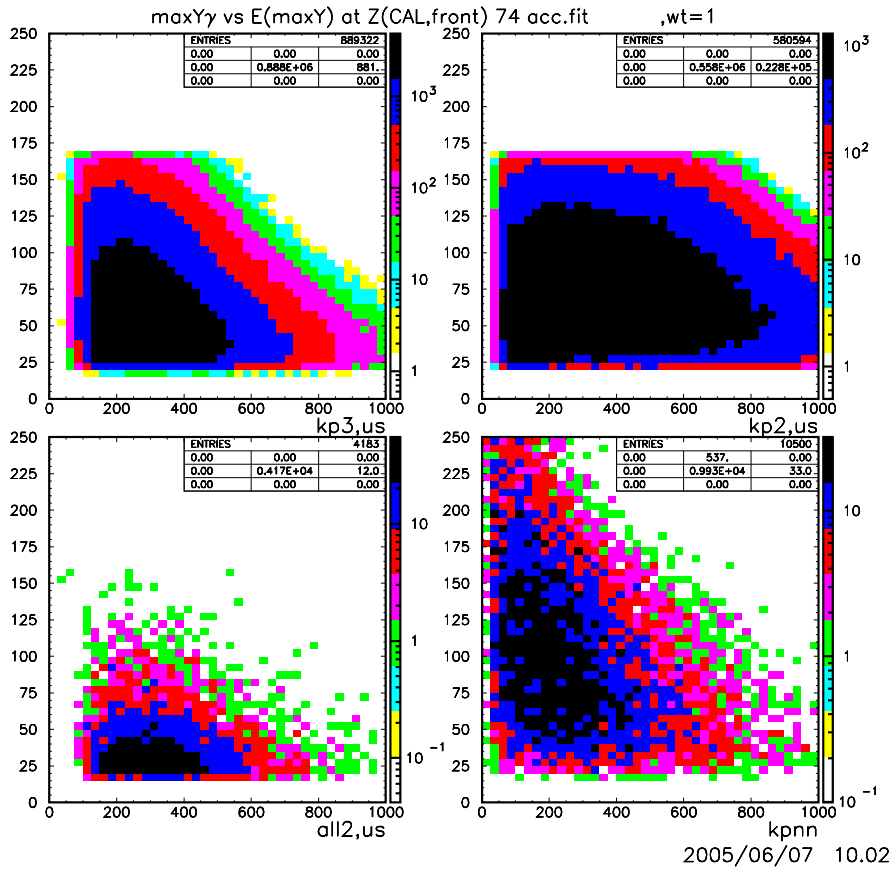


Figure 17: The energy of the photon with the maximum absolute y position extrapolated to the front of the calorimeter vs maximum absolute y position. The “GeomAcc” and “GoodFit” cuts have been applied. Top quartet: unit weights for all events. Bottom quartet: event weighting applied.

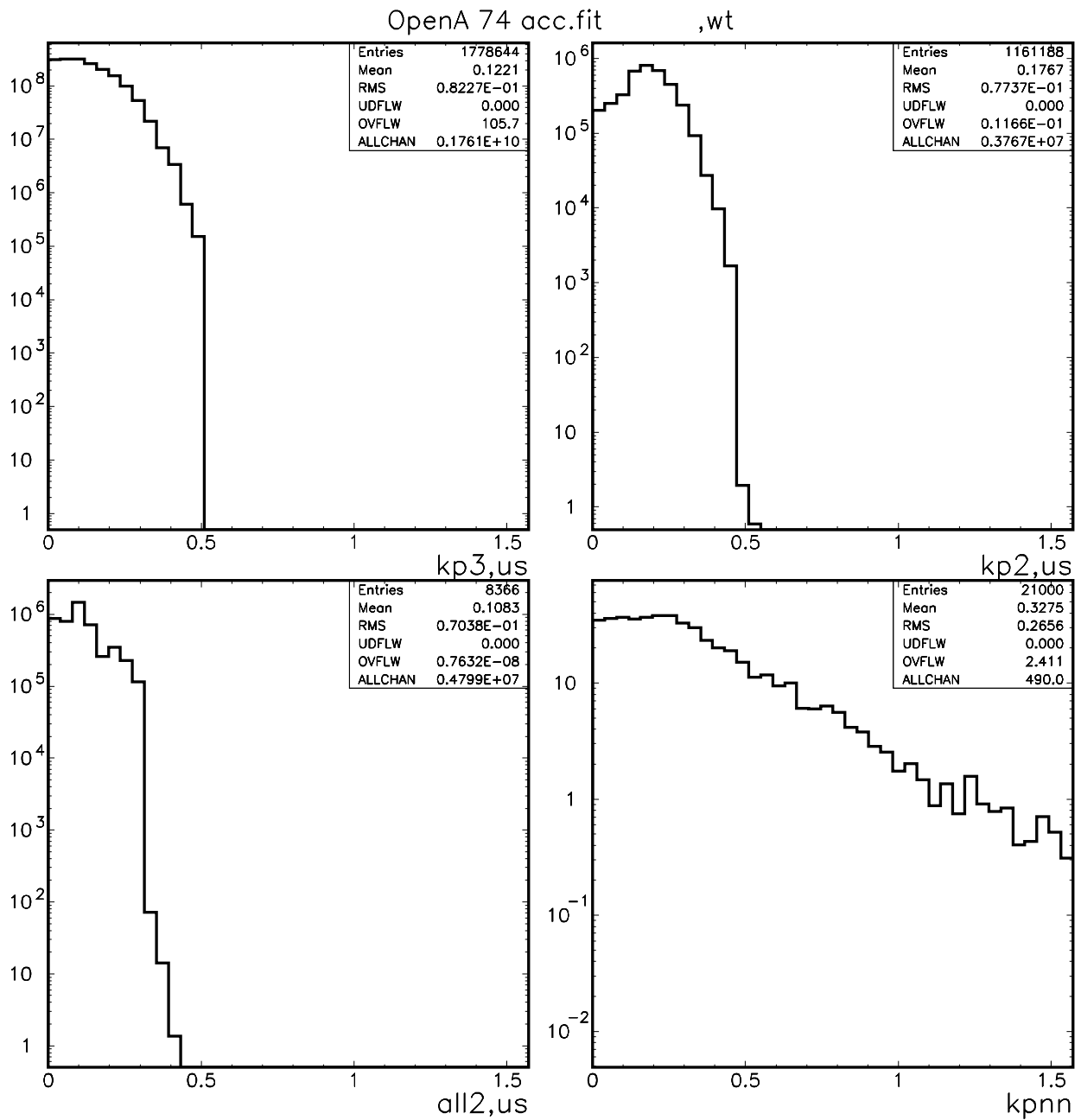


Figure 18: The expected number of events as a function of the measured opening angle between the two detected photons. The “GeomAcc” and “GoodFit” cuts have been applied.

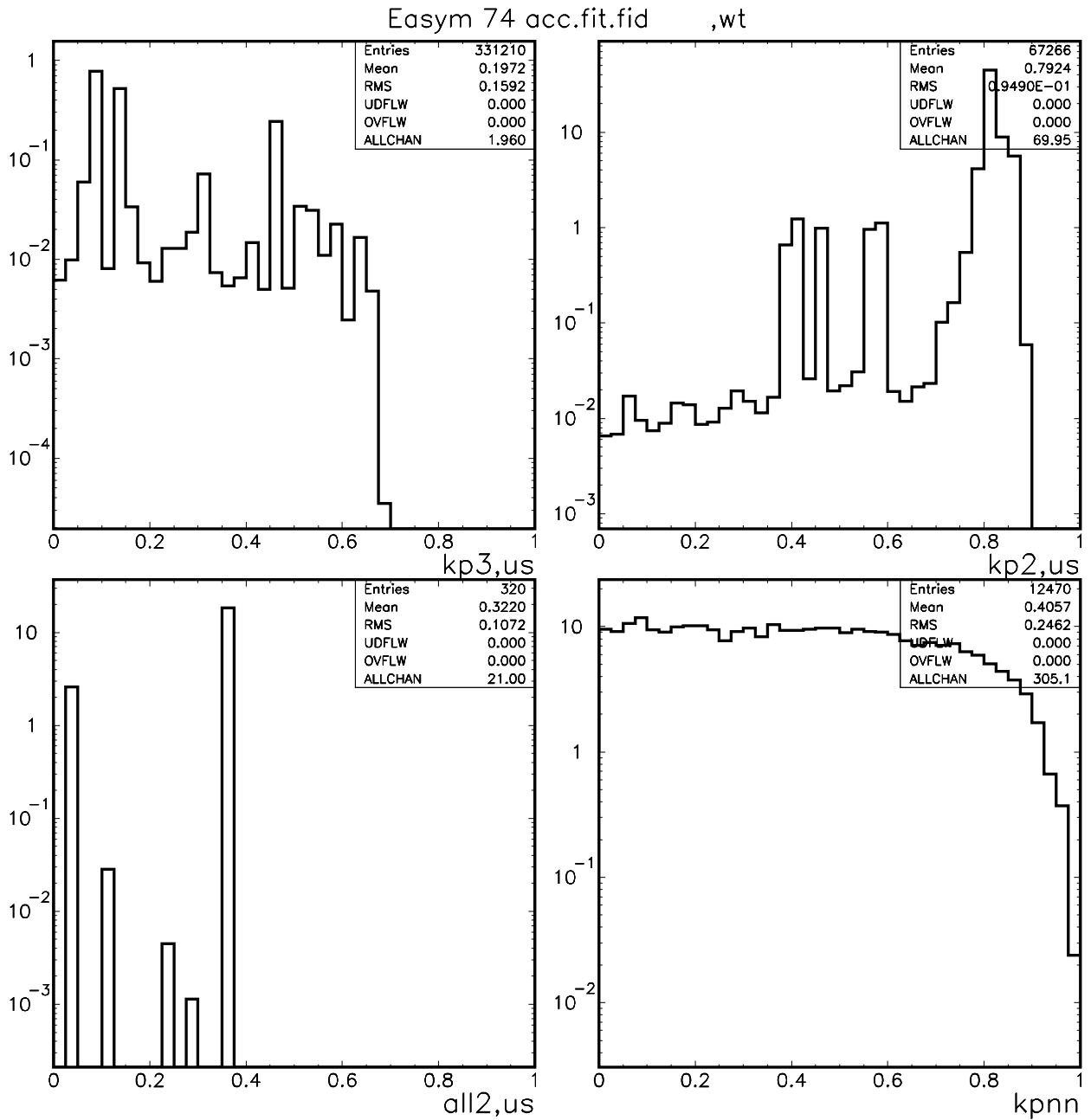


Figure 19: The expected number of events as a function of energy asymmetry \mathcal{A} of the two measured photons. $\mathcal{A} \equiv |E_1 - E_2|/(E_1 + E_2)$ where E_i is the measured energy of the i^{th} photon. The “GeomAcc”, “GoodFit” and “Fiducial” cuts have been applied.

Figure 20 shows the y separation vs the x separation between the two photons extrapolated to the z position at the US end of the calorimeter. The lower ‘band’ in y seen in the background corresponds to cases where the both photons are above or below the beam at the calorimeter. The upper ‘band’ corresponds to the case where one photon is above and the other photon below the beam. The y information shown in this Figure is another way of presenting the information in Figure 16 and discussed in Section 7 as an alternative to the YatCL cut.

In the FastMC, we can keep track of whether each photon was “smeared” with a narrow or wide gaussian to approximate the reconstructed angular resolution. As shown in Figure 21, after the “GeomAcc”, “GoodFit”, “Fiducial” and “MisRecon” cuts have been applied, the US background events are dominated by events where at least one of the photons was poorly measured (smeared by the wide gaussian) whilst approximately one-third (99/277) of signal candidates were poorly measured.

9 Discussion and summary

Mis-reconstruction of photon pairs from US K_L^0 decays that do not originate from a single π^0 decay can cause significant backgrounds. These backgrounds can be suppressed to a negligible level by a fiducial cut on the vertical conversion position of the photons in the PR. These backgrounds could also be suppressed by an additional veto located upstream of the UV. In addition, reduction in the tails in the reconstructed angles of the detected photons would also suppress this background. The current model of the PR [3] has no mechanism for identifying poorly reconstructed photons due to asymmetric e^+e^- pairs. An earlier PR model [4] showed that resolution tails could be reduced, with an attendant acceptance loss, by identifying poorly reconstructed photons due to asymmetric pairs. Certainly this should be one of the goals of a full-fledged reconstruction algorithm.

This note has not addressed background due to photons produced upstream of the decay region by other sources such as K_L^0 halo, neutrons interactions in the collimators, charged particle decays and interactions, etc. The geometric suppression afforded by a YatCL cut may be reduced because photons from these sources are not constrained to emanate from the well-defined beam envelope.

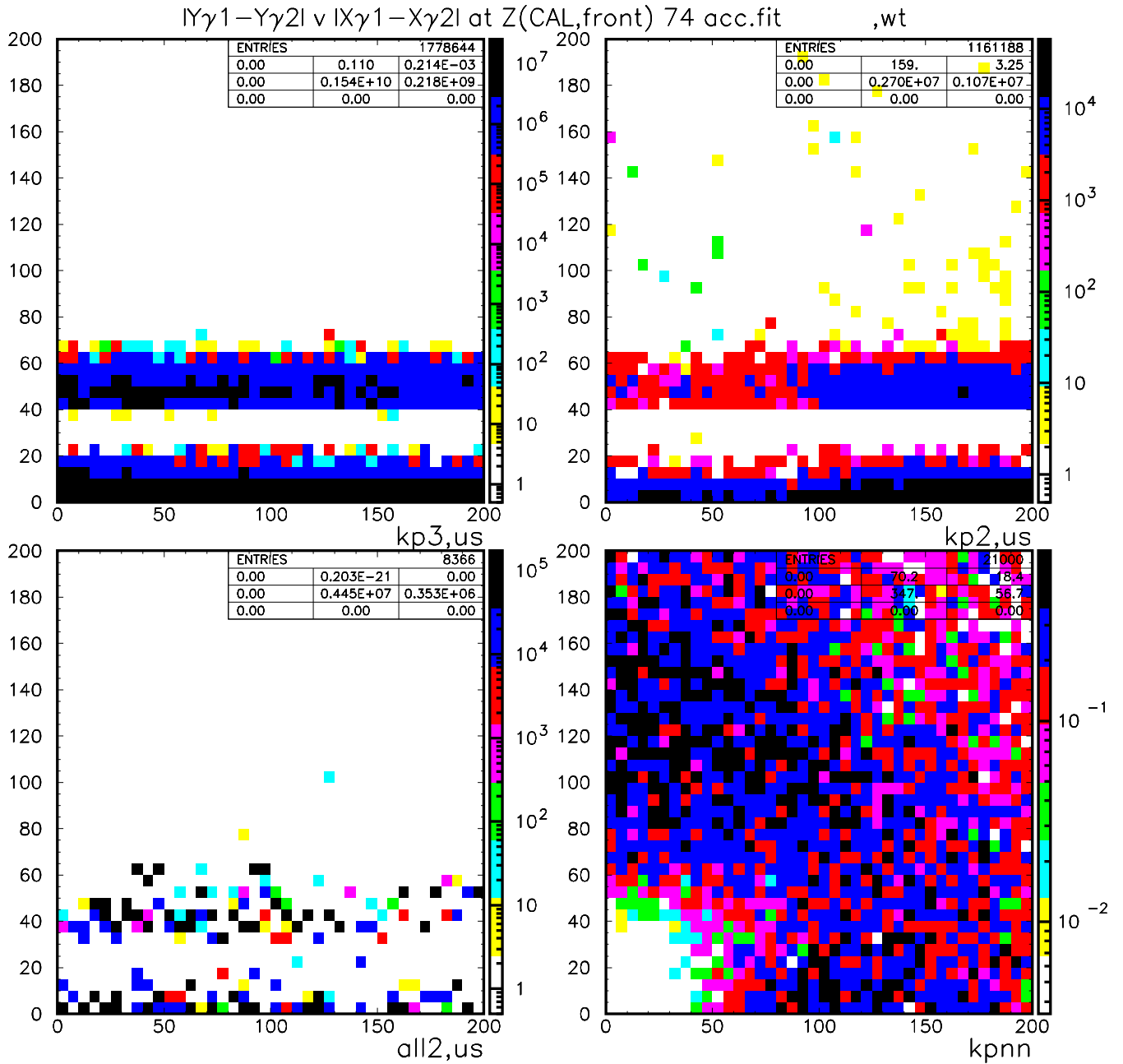


Figure 20: Δx vs Δy where $\Delta x \equiv |x_1 - x_2|$ is the magnitude of the difference reconstructed x positions of the two photons. Units are the expected number of events. The “GeomAcc” and “GoodFit” cuts have been applied.

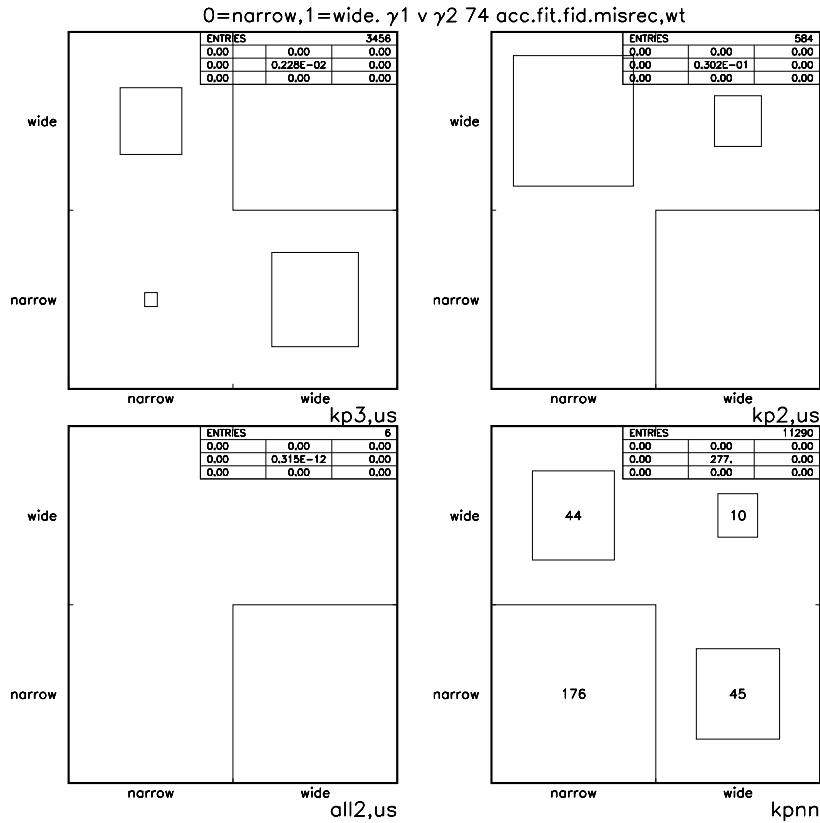
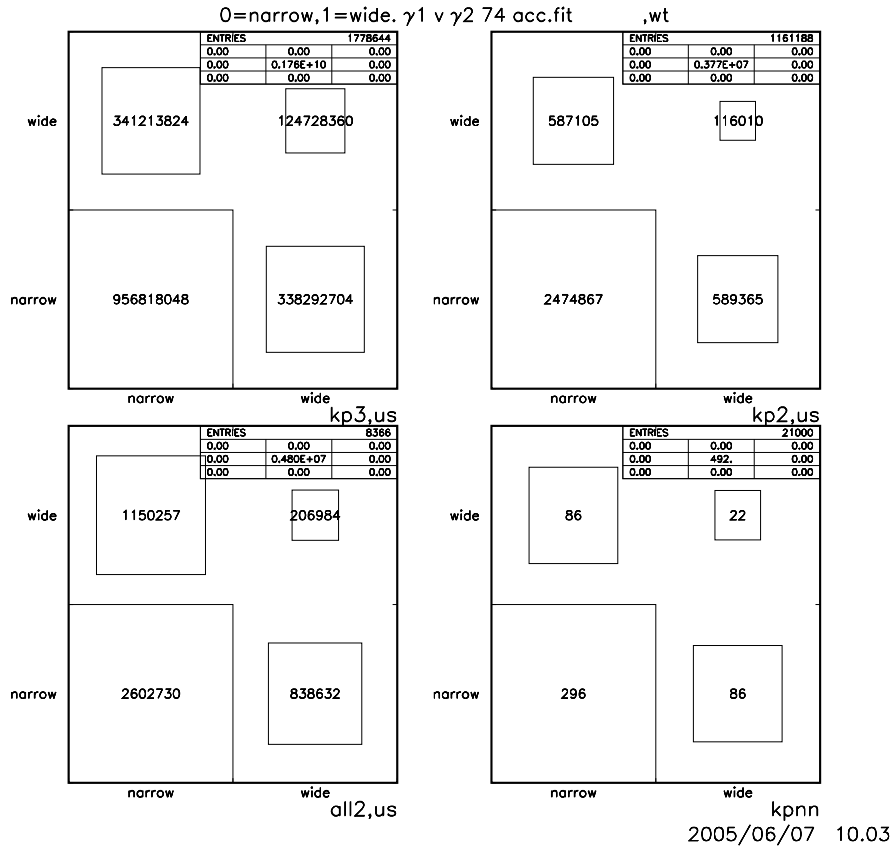


Figure 21: Photon resolution used to “smear” each hit. Units are the expected number of events. Size of box is proportional to the number of events. If < 1 events are expected, then nothing is written. Top quartet: The “GeomAcc” and “GoodFit” cuts have been applied. Bottom quartet: “GeomAcc”, “GoodFit”, “Fiducial” and “MisRecon” cuts have been applied.

10 Acknowledgements

I thank Dana Beavis, Laur Littenberg, Mike Marx and Carol Scarlett for helpful discussions. Doug Bryman pointed out how the conversion point in the PR would be useful. Doug, Andries van der Schaaf, Mike Zeller offered suggestions for other distributions to study.

References

- [1] D.E. Jaffe, *FastMC User Manual*, KOPIO TN089, 20 Oct 2004.
- [2] S. Kane, *Acceptance Ratios and Criteria*, KOPIO TN106, 20 Aug 04.
- [3] D. Bryman *E926 Preradiator Study: Alternating Horizontal and Vertical Anode Wires and Cathode Strips*, KOPIO TN014, 25 March 1999 and 14 April 2003 addendum,
- [4] M. Zeller, *A preradiator for E926 based on a Straw Tube design*, KOPIO TN006, 2 March 1998.